Journal of Vertebrate Paleontology 19(3):497–520, September 1999

CRANIOFACIAL ONTOGENY IN TYRANNOSAURIDAE (DINOSAURIA, COELUROSAURIA)

THOMAS D. CARR
Department of Palaeobiology, Royal Ontario Museum, 100 Queen's Park, Toronto, Ontario, M5S 2C6, Canada

ABSTRACT—A study of ontogenetic variation is used to clarify aspects of tyrannosaurid taxonomy and investigate the supposed phenomenon of dwarfism in the clade. A hypothetical ontogenetic trajectory is described for the relatively well-represented taxon *Albertosaurus libratus*. The type specimen of the purported "pygmy" tyrannosaurid *Nanotyrannus lancensis* was compared with specimens of *A. libratus* and found to share many morphological characters that exemplify immature specimens of the latter taxon. Most of the cortical surface of the Cleveland skull of *N. lancensis* has immature bone grain. Also, the skull shares unique derived characters with mature specimens of *Tyrannosaurus rex*, suggesting that the specimen is a young *T. rex* and not a dwarf tyrannosaurid. An increase in tooth width, accompanied by loss of tooth positions, and a global shift from an immature gracile to a mature robust morphotype in the craniofacial skeleton typifies the ontogenetic changes in *T. rex*. Similarly, on the basis of immature characters, *Maleevosaurus novojilovi* is considered to be an immature *Tarbosaurus bataar*.

INTRODUCTION

Since the turn of the century, articulated tyrannosaurid fossils have been recovered from Late Cretaceous sediments from western North America and central Asia. In particular, the Hell Creek (and equivalents) and Dinosaur Park formations of North America, and the Nemegt Formation of Mongolia, have yielded the greatest quantity of specimens including partial growth series for some taxa (Rozhdestvensky, 1965; Russell, 1970; Maleev, 1974).

In 1923, Matthew and Brown were the first to hypothesize immature features in a tyrannosaurid, the type specimen of *Gorgosaurus sternbergi* Matthew and Brown, 1922 (AMNH 5664), noting the lightly built jaws, slender muzzle, long and low maxilla, and round orbit. Despite its similarity to known specimens of *G. libratus* Lambe, 1914, the taxon was retained on the basis of its small size and slender proportions (Matthew and Brown, 1923).

Rozhdestvensky (1965) proposed that the holotype specimens of *Tarbosaurus efremovi* Maleev, 1955a, *Gorgosaurus lancinator* Maleev, 1955a, and *Gorgosaurus novojilovi* Maleev, 1955a, were ontogenetic variants of the same taxon, *Tarbosaurus bataar* Rozhdestvensky, 1965. He noted that young tyrannosaurids had slender jaws, an elongate tibia and metatarsal bundle, weakly developed limb joints, an elongate humerus, a columnar metatarsal III, and slightly different cranial proportions relative to older specimens. On the basis of this work, he suggested that *Gorgosaurus lancensis* Gilmore, 1946, is a young individual of *Tyrannosaurus rex* Osborn, 1905.

In 1970, Russell published a comprehensive review of tyrannosaurid taxa of western Canada. On the basis of the similarity of *Gorgosaurus* to *Albertosaurus* Osborn, 1905, the former genus was considered a subjective junior synonym of the latter. The holotype of *G. sternbergi* was recognized as a juvenile and referred to *A. libratus* (Russell, 1970). Russell identified limb proportions, degree of ossification of the pelvic bones and the skull roof, allometric changes in the skeleton, and the development of the nuchal crest and jugal cornual process as indicators of relative maturity among tyrannosaurids.

Based on a growth series of *T. bataar*, Carpenter (1992) observed that during ontogeny tyrannosaurid skulls deepen, the muzzle shortens, the orbit becomes dorsoventrally elongate, the supraorbital region of the skull becomes progressively rugose, the metatarsus shortens, and the neurocentral and calcaneoastragalar sutures fuse with age. Like Rozhdestvensky (1965), he implicated ontogenetic variation in Maleev's splitting of *T. bataar* into several taxa.

Despite these treatments of tyrannosaurid ontogeny and subsequent revisions of alpha taxonomy, consensus over the latter among workers is elusive (Bakker et al., 1988; Paul, 1988; Carpenter, 1992; Makovicky and Currie, 1998). Also, no study has documented the bone-by-bone changes in the tyrannosaurid craniofacial skeleton despite the wealth of material from the Dinosaur Park and Nemegt Formations. Documentation of size-independent morphological changes may facilitate the recognition of diagnostic and phylogenetically informative characters, thereby contributing to the resolution of the current lack of consensus over tyrannosaurid taxonomy.

Although gigantism characterizes derived tyrannosaurids (Bakker et al., 1988; Holtz, 1994a; Sereno, 1997), relative to other coelurosaur lineages, a complex and extensive phylogenetic history for tyrannosaurids is suggested by the identification of two dwarf forms, *Nanotyrannus lancensis* Bakker, et al., 1988 and *Maleevosaurus novojilovi* Carpenter, 1992. Although compelling from a macroevolutionary standpoint, the specimens upon which these taxa are based (CMNH 7541, PIN 552-2, respectively) have at some time been identified as distinct taxa (e.g., Maleev, 1955a; Gilmore, 1946; Russell, 1970; Bakker et al., 1988; Carpenter, 1992) or as juveniles of known taxa (e.g., Rozhdestvensky, 1965). Given the current knowledge of variation in tyrannosaurids, both interpretations are hypotheses of equal weight. Therefore, the issue invites investigation.

The purposes of this paper are: (1) to describe the ontogenetic changes in the skull bones of the well-represented taxon *Albertosaurus libratus*; (2) to describe taxonomic differences between taxa; and (3) to test the hypothesis of dwarf tyrannosaurids.

Institutional Abbreviations—**AMNH**, American Museum of Natural History, New York; **BHI**, Black Hills Institute of Geological Research, Inc., Hill City; **CMN**, Canadian Museum of Nature, Ottawa; **CMNH**, Cleveland Museum of Natural History; **FMNH**, Field Museum of Natural History, Chicago; **PIN**, Palaeontological Institute, Moscow; **ROM**, Royal Ontario Museum, Toronto; **TMP**, Royal Tyrrell Museum of Palaeontology, Drumheller; **UA**, University of Alberta, Edmonton; **USNM**, United States National Museum, Washington, D.C.

Published online 24 Aug 2010

TABLE 1. The 46 tyrannosaurid specimens examined first-hand for this study, with relative maturity specified.

Taxon	Relative maturity	Specimen number
Albertosaurus libratus	small Stage 1	CMN 2270, CMN 12063, TMP 85.11.3, TMP 86.144.1, TMP 94.12.155
	large Stage 1	AMNH 5432, AMNH 5664, ROM 436, ROM 1247, TMP 83.36.100, TMP 91.36.500
	Stage 2	AMNH 5336, CMN 2193, ROM 1422, ROM 4591
	Stage 3	AMNH 5458, CMN 2120
A. sarcophagus	—	AMNH 5222, CMN 5600, CMN 5601, ROM 12790, TMP 91.10.1, TMP 85.98.1, TMP 86.64.1
Daspletosaurus torosus	Stage 1	TMP 94.218.1
	Stage 4	AMNH 5346, CMN 841, CMN 8506, FMNH PR308, TMP 82.13.1, TMP 83.38.1, TMP 85.62.1
D. cf. *torosus*	Stage 1	CMN 11315
	Stage 2	MOR 590 (cast of maxilla)
Tyrannosaurus bataar	Stage 4	PIN 551-2 (cast)
T. rex	Stage 1	AMNH 5005, CMNH 7541
	Stage 2	AMNH 21542
	Stage 4	AMNH 5027, AMNH 5029, AMNH 5117, MOR 555 (cast), TMP 81.6.1, TMP 81.12.1, UCMP 118742 (cast)

METHODS AND MATERIALS

Materials

This study is based on observations and measurements of 46 tyrannosaurid specimens housed in several North American institutions (Table 1); all other specimens noted were observed from published photographs and figures. Tyrannosaurid cranial remains from the Dinosaur Park and Nemegt formations present a range from small (skull length 400 mm) to large (skull length 1,050+ mm) specimens. Skulls recovered from the Hell Creek Formation and equivalents are usually over 1 meter long, and only one small skull (skull length 572 mm) has been recovered to date.

Methods

The present analysis is descriptive, with an emphasis on the hypothetical ontogenetic changes to discrete morphological features. For comparison, teeth were measured mesiodistally and labiolingually at the crown base, immediately proximal to the distal carina. Terminology is after Bakker et al. (1988), Baumel and Witmer (1993), and Witmer (1997).

Following Bennett (1993) and Sampson (1993), cortical bone texture was used as a size-independent criterion of maturity where possible. Young ornithodirans are characterized by striated cortical bone that follows the direction of growth. Young tyrannosaurids also display striated cortical texture on virtually every bone. However, on many display specimens observation of bone texture was difficult or impossible to see given the distance imposed by glass cases and layers of consolidant or paint. Thus, a rigorous documentation of bone grain transition like that done for ceratopsids by Sampson (1993) could not be obtained.

Tyrannosaurids are unlike ceratopsids (Sampson, 1993) in their patterns of sutural fusion. In large tyrannosaurid specimens, fusion between endochondral (e.g., proötic, supraoccipital, otoccipital) occipital bones occurs, but without an evident pattern. Otherwise, the sutures between dermal and endochondral bones remain open. Sutural fusion may be an informative independent criterion for assessing relative maturity in tyrannosaurids, but in many of the specimens examined, sutures between braincase and occipital bones were obscured by glass cases, incomplete preparation, plaster restoration, or layers of consolidant.

In the present study, the hierarchically nested, progressive development of size-independent ontogenetic characters was used to identify ontogenetic stages. One young specimen, ROM 1247, was chosen for its completeness and immaturity (indicated by the presence of immature bone grain on each bone) for comparison with other *A. libratus* specimens. The specimen was described in detail as the reference for comparison with all other specimens. Features of other specimens that were less developed than those of ROM 1247 were considered immature; features showing greater development were considered more mature. For bones that were missing in ROM 1247 (e.g., postorbital, palatine, squamosal), specimens of the same ontogenetic stage (e.g., AMNH 5664) were used for comparison with other specimens for those bones.

On the basis of the changes of discrete morphological characters, the ontogeny of *A. libratus* was divided into three stages. Stage 1 specimens have (where observable) striated cortical bone grain and express nascent ontogenetic characters. One exceedingly small specimen (TMP 94.12.155), representing a skull of ~370 mm in length and consisting of a pair of mandibular rami, displayed features less developed than in the larger Stage 1 specimens. Since the entire skull was not represented, and only one informative character was noted, the specimen was not allocated to its own growth stage; ROM 1247 itself was regarded as a large Stage 1 specimen.

Stage 2 specimens exhibit development of the homologous features that typified Stage 1. Stage 2 specimens may also retain Stage 1 features, displaying a transitional constellation of characters between Stages 1 and 3. Stage 3 specimens express further development of the features that typified Stage 2 and display development of or retain Stage 1 features. Finally, Stage 4 is represented exclusively by adult *Daspletosaurus* and *Tyrannosaurus* specimens that display homologous ontogenetic features that are more developed than those of Stage 3 *A. libratus* specimens. The ontogenetic stages are of some degree arbitrary, but a quantitative analysis of the ontogenetic characters following Brochu (1996) is forthcoming to determine the relative maturity between individual specimens.

TAXONOMY OF DINOSAUR PARK AND HORSESHOE CANYON TYRANNOSAURIDAE

The holotype of *A. libratus* (CMN 2120) was first named *Gorgosaurus libratus* by Lambe (1914). Its slender upper incisiform teeth distinguished it from the robust dentition of *Deinodon horridus* Leidy, 1856 from the equivalent Judith River Formation of Montana. Later, Matthew and Brown (1922) showed that the type teeth of *Deinodon* and *Gorgosaurus* were indistinguishable, and that the two taxa likely were congeneric. However, the authors retained generic distinction in the absence of diagnostic skeletal material for *Deinodon.* Russell (1970), in agreement with Gilmore (1946), determined that the lectotype of *D. horridus,* comprising two incomplete incisiform teeth, is indistinguishable from the Dinosaur Park material, and *D. horridus* is therefore a nomen dubium (for an opposing view, see Sahni, 1972).

Russell (1970) concluded that *Gorgosaurus libratus* and *Albertosaurus sarcophagus* Osborn, 1905 were congeneric on the basis of overall similarity, a position that is upheld herein on a phylogenetic systematic basis (see Carr, 1996). *Albertosaurus*

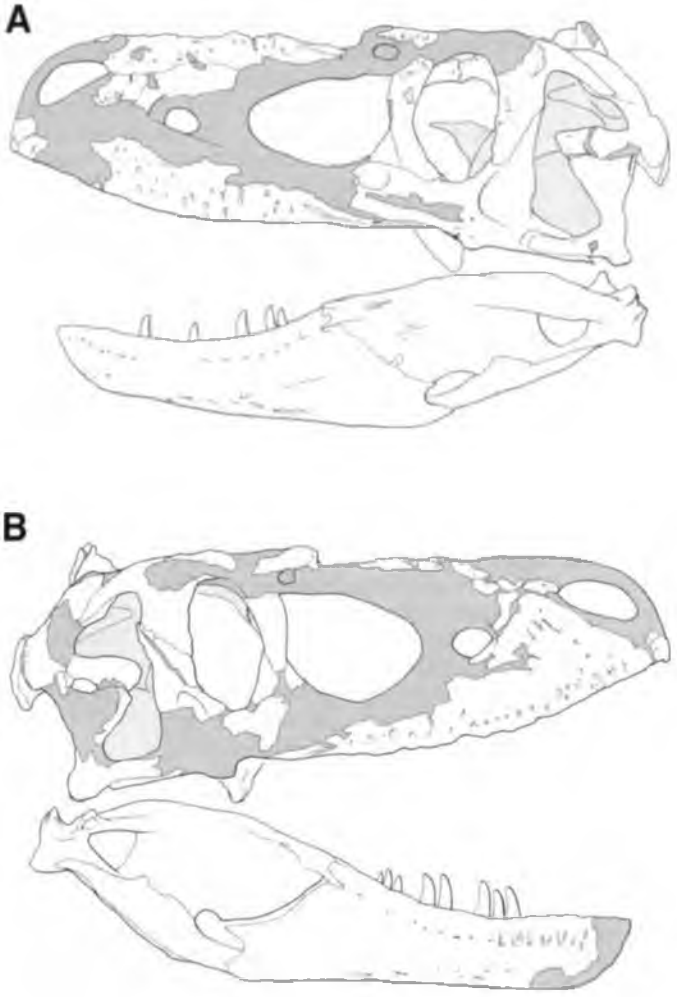

FIGURE 1. Relative completeness of the skull and jaws of FMNH PR308 (*Daspletosaurus torosus*) in left lateral (**A**) and right lateral (**B**) views. Skull length is 1,050 mm.

was rediagnosed and distinguished from *Daspletosaurus* by Russell (1970).

I agree with Russell (1970) that the types and referred material of *G. libratus* and *A. sarcophagus* appear to be identical, and are different from specimens referred to *Tyrannosaurus bataar* Maleev, 1955b and *T. rex* Osborn, 1905. I also agree with Carpenter (1992) that discrete differences exist between the tyrannosaurid skulls from the Dinosaur Park and Horseshoe Canyon formations.

Ontogenetic changes to discrete morphological characters are based on specimens referred to *A. libratus,* with the exception of FMNH PR308. Morphologically, this specimen is identical to the morphotype represented by *D. torosus.* Although the skull is considered representative of *A. libratus* (Russell, 1970: fig. 1; Paul, 1988:335; Carpenter, 1992:figs. 1, 2E), the specimen is less complete (Fig. 1A, B) than usually shown. Also, FMNH PR308 has been focal in discussions of tyrannosaurid diversity, with specific reference to tooth size and number (Bakker et al., 1988; Paul, 1988). In fact, every upper tooth and all but 13 dentary teeth are restored in plaster (pers. obs.), rendering the material basis of the former aspect moot.

The relationship between size and morphology has not been adequately studied in large theropods, and no attempt has been made to do so herein. This important question would best be answered by a quantitative and comparative study in the realms of biomechanics and functional morphology. The ontogenetic characters in this study were chosen cognizant of this issue. Thus, inclusive features of possible structural importance to the skull were avoided.

TAXONOMY OF NEMEGT TYRANNOSAURIDAE

I agree with Paul (1988) and Carpenter (1992) that *Tarbosaurus* is a junior subjective synonym of *Tyrannosaurus* (contra Rozhdestvensky, 1965). Both species are united by the absence of a lacrimal horn (Carpenter, 1992), inflated descending paroccipital process, transversely-oriented occipital plate, and rostrocaudally restricted basisphenoid recess, among other features. A more detailed treatment of tyrannosaurid systematics is forthcoming.

DESCRIPTION

Ontogenetic Variation in *Albertosaurus libratus*

Premaxilla—The premaxilla of Stage 1 specimens of *A. libratus* is transversely narrow with a concave lateral margin, has a shallow alveolar process (Fig. 5A), narrow maxillary process (Fig. 5C), and the maxillary articular surface of the alveolar process is transversely narrow. The premaxillae of Stage 2 specimens are not distinctive. In Stage 3 specimens, the premaxillae are transversely broad in rostral view, which straightens the lateral margin of the bone.

Maxilla—In small Stage 1 specimens (e.g., CMN 12063) of *A. libratus,* the maxilla is transversely compressed. In large Stage 1 specimens (e.g., ROM 1247) in lateral view, the bone is thickened, and the slot for the maxillary process of the nasal is dorsolateral in position (1; Fig. 2E). In small Stage 1 specimens, the margin of the antorbital fossa is sharply delimited, and its ventral margin may pass caudally in a concave arc, or is straight; in larger specimens, the rostroventral margin of the fossa grades into the textured bone surface (2; Figs. 2E, 5A). In small specimens, the base of the interfenestral strut is flat, but is gently concave in large specimens (3; Figs. 2E, 5A).

In Stage 1 specimens, the antorbital fenestra is longer than high (Fig. 5A). The lateral surface is textured and incised by shallow neurovascular sulci, the ventral margin of the antorbital fossa is bounded by a low ridge (4), and the alveolar process is shallow (5; Figs. 2E, 5A). The vestibular bulla and passage of the subnarial foramen are laterally flat or transversely convex (6; Fig. 2E).

Also in Stage 1 specimens, the rostroventral foramen of the premaxillary process is small and the rostrodorsal foramen is a cleft-like, ventrally opening slit (Fig. 5A). The caudal foramen of the ventral row of foramina bears a caudal elongate sulcus, that does not leave the ventrolateral margin of the jugal process (7; Figs. 2E, 5A). The maxillary fenestra is positioned midway between the rostral margins of the antorbital fenestra and fossa, and is as long as deep or barely longer than high (8; Figs. 2E, 5A). The lateral surface separating the antorbital fossa and nasal suture is a shallow tab (9; Figs. 2E, 5A). Finally, the promaxillary fenestra is a slit-like foramen within the rostral margin of the antorbital fossa (10; Figs. 2E, 5A) (Russell, 1970).

In Stage 2 specimens (e.g., AMNH 5336), the maxilla is thickened laterally and bowed rostrally (11; Fig. 2F). The rostrolateral surface is expanded rostrally and dorsoventrally (Fig. 2F) and its surface sculpturing is pronounced. The ventral margin of the antorbital fossa is either gently sigmoid or dorsally convex (Fig. 2F). The depression ventral to the antorbital fossa is shallow (12; Fig. 2F). The maxillary fenestra is longer than high and approaches the rostral margin of the antorbital fenestra (13; Fig. 2F). The promaxillary fenestra is recessed dorsally (14), and the lateral surface of the maxilla passes over the ros-

tral margin of the antorbital fossa as a strut (15; Fig. 2F). The rostroventral foramen of the premaxillary process is larger than the round rostrodorsal foramen. The ventral rim of the ventral jugal process is breached by the sulcus from the caudal foramen of the ventral row of foramina (16; Fig. 2F).

In Stage 3 specimens (e.g., AMNH 5458), the rostrolateral surface of the bone is thickened, bowed, and expanded, displacing the articular surface for the nasal dorsally. The rostrolateral foramina are enlarged. The base of the interfenestral strut is concave, and the height of the antorbital fenestra approaches its length.

In medial view in *A. libratus,* shallow pneumatic excavations are present in the maxillary antrum in Stage 1 specimens (e.g., ROM 1247; Fig. 2I). The caudoventral excavation may be shallow or pocket-like (17; Fig. 2I). The floor of the promaxillary antrum is crossed by a low ridge above the third alveolus. The palatal process has a strong rostrodorsal sigmoid curvature (18); its caudal surface is flat such that its dorsal surface is visible (19) and its ventral margin extends beneath the level of the medial alveolar process (20; Figs. 2I, J). The medial edge of the palatal process is cleaved by the articular surface for the palatine (21; Figs. 2I, J). Also, the palatal process is transversely narrow; the tooth root bulges are low (22; Fig. 2J), and the interdental depressions are shallow.

Nasal—In Stage 1 specimens (e.g., ROM 1247) of *A. libratus,* the nasal is lightly built, and moderately or strongly vaulted rostrally (Figs. 2B, C, 5A, C). The caudal plate expands slightly between the lacrimals (25; Figs. 2B, C, 5C). The lacrimal articular facet overlaps the dorsolateral edge of the bone (26; Figs. 2B, C, 5C). The dorsal surface of the nasal is irregular and bears rugosities, cusps, and bony papillae that interrupt the dorsal row of neurovascular foramina (Fig. 5C).

In Stage 2 specimens (e.g., ROM 4591), the nasal is thickened rostrally and the ventral surface is not strongly vaulted. The caudal plate expands between the lacrimals. The medial frontal process may be absent in Stage 2 specimens (e.g., AMNH 5336). In Stage 3 specimens, the lateral margins of the caudal plate expand or are parallel (e.g., CMN 2120) between the lacrimals.

Lacrimal—In small Stage 1 specimens (e.g., TMP 86.144.1) of *A. libratus,* the ventral process of the rostral ramus is absent (Fig. 3A); in larger specimens (e.g., ROM 1247), the ventral process is incipient (25; Fig. 3B, 5A). In small Stage 1 specimens, the cornual process is a weak ridge with three apices and is shallower than the lacrimal pneumatic recess (26; Fig. 3A). In large Stage 1 specimens, the cornual process projects rostrodorsally, bears two apices, and is as deep or deeper than the lacrimal pneumatic recess (27; Figs. 3B, 5A). The lacrimal of Stage 1 specimens is T-shaped, with the supraorbital ramus projecting strongly behind the ventral ramus (28; Figs. 3A, B; 5A). In larger specimens, the rostrolateral margin of the cornual process is eave-like, and dished above the lacrimal pneumatic recess (29; Figs. 3B, 5A). In large Stage 1 specimens the dorsolateral surface of the supraorbital ramus bears a strong shelf-like ridge (30; Figs. 3B, 5A).

In small Stage 1 specimens, the rostral ramus is divided into lateral and medial processes; the former is situated dorsal to the latter, so that the ramus is forked in lateral view (31; Fig. 3A). In larger Stage 1 specimens, the processes overlap in lateral view, losing the forked appearance (32; Fig. 3B). In small specimens, the lacrimal antorbital fossa of the dorsal ramus is fully exposed to view (33; Fig. 3A). In larger specimens, the lateral external surface is extruded ventrally as a lamina, partly concealing the fossa in lateral view, creating a slot-like passage (31; Figs. 3B, 5A).

In Stage 1 specimens, the textured dermal surface and the smooth fossa surface merge at their juncture (32; Fig. 2A). In Stage 1 specimens, the rostral margin of the ventral ramus merges with the ventral lip of the lacrimal antorbital fossa (33; Fig. 3A, B, 5A). Also, the rostral margin of the rostroventral lamina of the lacrimal is straight or concave in lateral view (34; Figs. 3A, B, 5A). The jugal articular surface of the rostroventral lamina exceeds that of the ventral ramus. The caudal margin of the jugal articular surface of the ventral ramus is subvertical (Fig. 5A).

In Stage 2 specimens (e.g., AMNH 5336), the ventral process of the rostral ramus is developed, but is shorter than the dorsal process (35; Fig. 3C). The cornual process may be bulbous and has one apex (36; Fig. 3C). The ventral margin of the lateral lamina of the rostral ramus matches that of the lacrimal antorbital fossa (37; Fig. 3D). The caudal margin of the jugal articular surface of the ventral ramus slopes caudodorsally (38; Fig. 3E). This is also in *D. torosus* (39; Fig. 3H) The rostral margin of the ventral ramus is embayed by the lacrimal antorbital fenestra (40; Fig. 3C).

In Stage 3 specimens (e.g., CMN 2120), both the dorsal and ventral processes of the rostral ramus are elongate (41; Fig. 3E). The cornual process bears a single erect apex, situated above the ventral ramus (42; Fig. 3E). The lateral surface around the lacrimal pneumatic recess is not dished (43; Fig. 3E). The lacrimal antorbital fossa is attenuated rostrally by the lateral lamina (44; Fig. 3E). This condition is also seen in Stage 4 *D. torosus* (45; Fig. 3G) and *T. rex.* In *A. libratus,* it is equivocal whether or not the lateral and medial laminae are fused ventrally; the specimen in which this is observed (CMN 2120) is mediolaterally crushed in this region (Fig. 3E).

In Stage 3 specimens (e.g., AMNH 5458), an edge separates the rostral margin of the ventral ramus from the lacrimal antorbital fossa. The rostral margin of the rostroventral lamina is convex in lateral view (46; Fig 3E) and the extent of its contact with the jugal is matched by that of the ventral ramus (47; Fig. 3E). This is also in Stage 4 *D. torosus* (Fig. 3F).

Jugal—In small Stage 1 specimens (e.g., TMP 86.144.1) of *A. libratus,* the postorbital ramus is caudodorsally declined. In Stage 1 specimens (e.g., ROM 1247), the orbital margin is low and elongate (48; Fig. 3I) and the maxillary ramus of the jugal is straplike and shallow (49; Fig. 3I). In larger Stage 1 specimens, the jugal pneumatic recess is a transversely narrow slit (Fig. 5A, C); its caudal edge may be united with that of the lacrimal (50; Russell, 1970) (Figs. 3I, 5A). Infrequently, the caudal margin of the recess may be resorbed, exposing the rostral extent of the secondary fossa to lateral view (51; Figs. 3I, 5A).

The caudal margin of the lacrimal articular surface is subvertical in lateral view (52; Figs. 3I, 5A). The articular surface for the postorbital is shallow and extends to the ventral orbital margin (53; Figs. 3I, 5A). The medial articular surface for the lacrimal is overlapping. The caudal margin of the postorbital ramus is sinuous or concave (54; Figs. 3I, 5A). The area ventral to the postorbital ramus is flat or convex in lateral view (55; Figs. 3I, 5A). The transversely flat cornual process may be pronounced or its caudal margin may be low (56; Figs. 3I, 5A). Finally, the quadratojugal articular surface passes rostrodorsally at or caudal to the midlength of the ventral process of the quadratojugal ramus, either horizontally or at a steep angle (57; Figs. 3I, 5A).

In Stage 2 specimens (e.g., AMNH 5336), the postorbital articular surface ends above the ventral margin of the orbit (58; Fig. 3J), the caudal margin of the postorbital ramus is strongly convex or straight at midheight (59; Fig 3J), and the cornual process is pronounced (60; Fig. 3J).

In Stage 3 specimens, the maxillary ramus is dorsoventrally deep (61; Fig. 3K). The caudal margin of the jugal foramen is resorbed, exposing the rostral margin of the secondary fossa (62; Fig. 3K). The lateral surface at the base of the postorbital ramus is shallowly concave (63; Fig. 3K). The caudodorsal

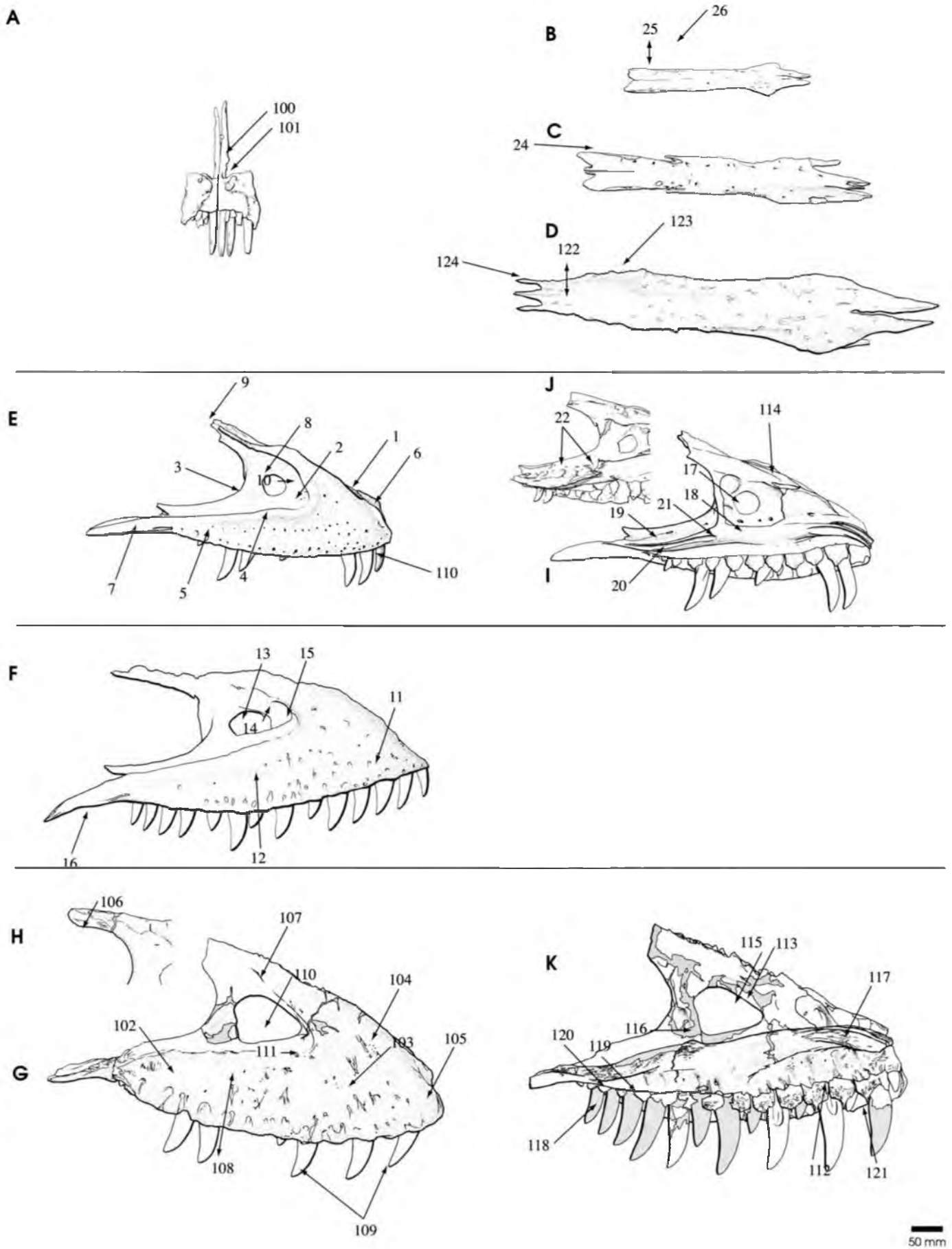

FIGURE 2. Growth series of *Albertosaurus libratus* craniofacial bones: nasals in dorsal view (TMP 86.144.1, **B**; ROM 1247, **C**); maxillae in lateral (ROM 1247, **E**; AMNH 5336, **F**) and medial (CMN 12063, **J**; ROM 1247, **I**) views. Craniofacial bones of *Daspletosaurus torosus*: premaxilla (CMN 8506, **A**); nasals (CMN 8506, **D**) in dorsal view; maxilla in lateral (CMN 8506, **G**; AMNH 5346, **H**) and medial (CMN 8506, **K**) views. Arrows indicate features discussed in text. Bones have been reversed to face right when required. Scale bar equals 50 mm; **F** is not to scale.

margin of the jugal pneumatic recess merges with the lateral surface of the jugal beneath the lacrimal contact (64; Fig. 3K). Finally, the caudal margin of the lacrimal articular surface slopes caudodorsally along an elongate and shallow lateral overlap (65; Fig. 3K).

Postorbital—In lateral view, the postorbital of small Stage 1 specimens of *A. libratus* is a slender and delicate bone (Fig. 3M). The frontal ramus approaches the length of the squamosal and jugal rami (66; Fig. 3M). The squamosal ramus is slender and arched in lateral view (67; Fig. 3M). The cornual process is a low, striated depression at the caudodorsal margin of the orbit (68; Fig. 3M). The jugal ramus is elongate and slender (69; Fig. 3M), and the jugal articular surface is shallow. The lateral surface of the jugal ramus bears dorsally arched sulci (70; Fig. 3M). The rostral and caudal margins of the jugal process are parallel in lateral view (71; Fig. 3M) and reach the ventral margin of the orbit. In dorsal view, the dorsotemporal fossa is shallow and is not bounded rostrally by a ridge.

In large Stage 1 specimens, the ventral margin of the squamosal process is sinuous (72; Fig. 3N). In Stage 1 specimens, the dorsal margin of the bone tends to be vertically oriented (Fig. 5C). In large Stage 1 specimens, the incipient cornual process is a flattened, ear-like tab of bone with a horizontal ridge beneath its dorsal margin (75; Fig. 3N). The dorsally-arched sulci reach its rostral and caudal margins (74; Fig. 2P). The squamosal articular surface extends forward of the rostral margin of the laterotemporal fenestra. The frontal ramus is short in lateral view (76; Fig. 3N), and is broad in dorsal view with a moderately deep dorsotemporal fossa bounded by a low ridge rostrally.

In Stage 2 specimens, the sulci of the jugal ramus are restricted rostral to its caudal margin (77; Fig. 3O). The laterodorsal bone margin is everted medially (78; Fig. 3O) and the bone ends above the orbit floor. The frontal ramus is stout and deep in lateral view (79; Fig. 3O). The cornual process is prominent (80). In Stage 3 specimens, the cornual process of the postorbital may be enlarged, consisting of a thick ridge separated by a deep crease from an enlarged caudoventral boss. This is also true for *D. torosus* (81; Fig. 3P).

Frontal—In large Stage 1 specimens (e.g., ROM 1247) of *A. libratus,* the orbital margin is within a vertical slot between the articular surfaces for the lacrimal and postorbital in lateral view (Figs. 5A, C). The lacrimal notch is long and narrow in dorsal view (Fig. 5C). The paired frontals are longer than wide (Fig. 5C). In Stage 1 specimens, the dorsotemporal fossa is shallow (Fig. 5C). In Stage 2 specimens (e.g., AMNH 5336), the fossa is deep. In Stage 1 specimens, the frontals are flattened to meet at the midline (Fig. 5C). In Stage 2 specimens, the frontals slope dorsomedially to their contact.

In Stage 1 specimens (e.g., ROM 1247) of *A. libratus,* the prefrontal articular surface is narrow in dorsal view.

Parietal—In Stage 1 specimens (e.g., ROM 1247) of *A. libratus,* the nuchal crest is low in caudal view, only as deep as the dorsal process of the supraoccipital. The rostrodorsal surface of the crest is rugose laterally and the dorsolateral margin of the crest flares caudolaterally (Fig. 5C). The sagittal crest is low (Fig. 5A).

In Stage 2 specimens (e.g., AMNH 5336), the rostrodorsal margin of the nuchal crest is rugose to the midline and the dorsolateral margin is rugose caudally. The dorsal margin of the sagittal crest is concave in lateral view. In Stage 3 specimens (e.g., AMNH 5458), the nuchal crest is tall, twice as deep as the dorsal process of the supraoccipital.

Basioccipital—In Stage 1 specimens (e.g., ROM 1247) of *A. libratus,* the occipital condyle is caudoventrally flattened and the lateral margins converge ventrally. The ventral surface of the basituberal web is flat and arches dorsally in caudal view. The surface beneath the occipital condyle is convex in frontal section and flares ventrally between the ascending scars (sensu Bakker et al., 1988). Finally, the basal tuber is poorly developed.

In Stage 2 specimens (e.g., AMNH 5336), the occipital condyle is spherical. The basal tuber forms a rugose block. In Stage 3 specimens (e.g., AMNH 5458), the caudal surface of the basioccipital is concave ventral to the occipital condyle.

Basisphenoid—In Stage 1 specimens (e.g., ROM 1247) of *A. libratus,* the basipterygoid process is flattened rostrolaterally, the basisphenoid pneumatic foramina are small and set above the ventral margin of the basipterygoid web. In lateral view, the ventral margin of the bone slopes at a low rostroventral angle such that the dorsal margin of the basipterygoid process does not project below the level of the caudoventral corner of the bone. The oval scar (sensu Bakker et al., 1988) is smooth, ventromedially oriented, and narrow.

In Stage 2 specimens (e.g., AMNH 5336), the oval scar is broad. In Stage 3 specimens (e.g., AMNH 5458), the ventral margin of the basisphenoid descends steeply rostroventrally in lateral view such that the dorsal margin of the basipterygoid process extends ventral to the level of the caudoventral corner of the bone. The oval scar is laterally expanded, ventrally oriented, and dished.

Vomer—In lateral view, the vomer of Stage 1 specimens (e.g., ROM 1247) of *A. libratus* has a horizontal ventral margin which curves gently caudoventrally, caudal to midlength (83; Fig. 4A). A slender neck is present between the transversely-expanded maxillary process and the dorsally deep body of the bone (82; Fig. 4A). In Stage 2 specimens (e.g., AMNH 5336), the ventral margin curves strongly caudoventrally behind the midlength of the bone.

Palatine—In small Stage 1 specimens (e.g., TMP 86.144.1) of *A. libratus,* the caudalmost of the two pneumatic recesses in the lateral surface of the bone is rostrocaudally elongate and vertical struts are present on the medial wall of the rostral recess. The septum between the pneumatic recesses is narrow. Also, the palatine body is transversely compressed. In larger Stage 1 specimens (e.g., USNM 12814), the palatine is transversely inflated. In small Stage 1 specimens, the vomerine ramus is dorsoventrally shallow in lateral view; it is deep in larger Stage 1 specimens.

Surangular—In small Stage 1 specimens (e.g., TMP 86.144.1) of *A. libratus,* there is no ridge lateroventral to the glenoid in lateral view and the caudal margin of the retroarticular process is concave. In small and larger Stage 1 specimens (e.g., ROM 1247), the bone is shallow, such that the rostroventral margin is convex and slopes at a low angle caudoventrally (84; Figs. 4E, 5B). The intramandibular process is stout and deep, its ventral margin meets the rostroventral margin of the bone along a shallow curve, or is confluent (85; Figs. 4E, 5B). The rostral plate is externally flat (86; Figs. 4E, 5B). The surangular shelf slants rostroventrally (87; Figs. 4E, 5B) or horizontally; its lateral margin projects laterodorsally. The dorsomedial flange may be low and blade-like (88) or high (TMP 86.144.1) with a narrow shelf separating it from the surangular shelf, in which the insertion scar of M. adductor mandibulae externus (Molnar, 1991) is indistinct and confined medial to the surangular shelf (Figs. 4E, 5B).

In large Stage 1 specimens (e.g., ROM 1247), the surangular foramen is not deeply recessed caudodorsally (89; Figs. 4E, 5B). The fossa ventrolateral to the glenoid is shallow and smooth (90; Figs. 4E, 5B). The caudal margin of the retroarticular process is straight to convex, such that the flange for the articular is weakly developed (Figs. 5B).

In Stage 2 specimens (e.g., AMNH 5336), the bone is deep such that the rostroventral margin slopes at a steep angle caudoventrally. The ventral margin of the intramandibular process and rostroventral margin of the surangular meet at an angle.

The surangular shelf passes horizontally, rostroventrally, or rostrodorsally, and its lateral margin projects horizontally. The surangular foramen is large and recessed. The sulcus lateroventral to the glenoid is dorsoventrally deep and rugose.

In Stage 3 specimens (e.g., CMN 2120), the intramandibular process is elongate and meets the rostroventral margin at an angle (91; Fig. 4F). The surangular shelf passes rostrodorsally (92; Fig. 4F) and the dorsomedial process is tall. The dorsolateral muscle scar is delimited rostrally by a sharply inset facet, which extends to the lateral surface of the surangular shelf (93; Fig. 4F). The caudal margin of the retroarticular process is concave.

Prearticular—In small Stage 1 specimens (e.g., TMP 86.144.1) of *A. libratus,* the ventral portion of the articular surface of the angular is reduced and the lateral surface of the contact is aliform. In Stage 1 specimens (e.g., ROM 1247), the dorsal margin of the caudal ramus is restricted caudally (94; Fig. 4J). The caudal ramus is shallow with parallel dorsal and ventral margins (95; Fig. 4J). The rostral lamina is strap-like (96) and pointed distally (97); its caudodorsal margin is smooth (Fig. 4J). In large Stage 1 specimens, the angular facet is flat and not aliform.

In Stage 3 specimens (e.g., CMN 2120), the dorsal margin of the caudal ramus, with the adductor attachment surface, is shifted rostrally toward the mid-shaft (98; Fig. 4K). The caudal ramus is deep such that the dorsal and ventral margins are gently convex and converge rostrally (99; Fig. 4K). The caudodorsal margin of the rostral lamina bears a rugose surface for muscle attachment.

Dentary—In small Stage 1 specimens (TMP 94.12.155) of *A. libratus,* the shallow dentary is as wide as it is deep. In larger Stage 1 specimens (e.g., ROM 1247), the dentary is deeper than wide. The angular process is dorsoventrally shallow (Fig. 5B). The symphyseal facet is flat and textured by stout caudodorsal bony papillae. The splenial articular surface is indicated by light, arcuate rostroventral ridges. The ventral bar beneath the Meckelian foramen is lightly rugose and rostroventrally excavated by a broad sulcus. Usually in tyrannosaurids the angular process is bifurcated by the external mandibular fenestra in lateral view; in ROM 1247 (Fig. 5B) this emargination is absent on both sides. In Stage 2 specimens (e.g., AMNH 5336), the angular process is deep. In Stage 3 specimens (e.g., AMNH 5458), the symphyseal surface may be rugose.

Taxonomic Variation

Premaxilla—In rostral view, the premaxillae of the holotype (Stage 4) of *D. torosus* (CMN 8605) are fused by struts of bone at the base of the nasal process; however, it is possible that the trabeculae are pathological exostoses. In addition, "skirts" of bone extrude from the external margin of the alveoli, and the alveolar process is deep (see Appendix 1 for a synoptic comparison of taxonomic variation).

In caudal view (Fig. 2A), the medial process of the premaxilla of *D. torosus* has a pronounced dorsal flange (100), and there is a crest-like ridge that delimits the subnarial foramen ventrally (101; Fig. 2A). In *D. torosus* and Stage 4 *T. rex* specimens, the maxillary process is broad, elongate, and flattened (Fig. 8C, I). In *T. rex* the maxillary process broadly overlaps the medial edge of the maxillary process of the nasal.

Maxilla—In lateral view in Stage 4 specimens of *D. torosus* (e.g., CMN 8506), the maxilla is thickened transversely, eliminating the depression ventral to the antorbital fossa, and the ventral floor of the fossa is ledge-like (102; Fig. 2G). The lateral surface sculpture is pronounced, with deep neurovascular sulci (103; Fig. 2G). The nasal articular surface is displaced medially (104; Fig. 2G). The vestibular bulla is swollen and convex in transverse section (105; Fig. 2G) and its foramina are separated by the rugose lateral surface. The lateral surface separating the antorbital fossa from the nasal suture is as deep as the fossa beneath it (106; Fig. 2H). The articular surface for the nasal may be transversely broad, forming a deep peg-and-socket articulation (107; Fig. 2G, K).

The alveolar process of the maxilla in *D. torosus* is deep and expanded; the dorsal and ventral margins gradually converge caudally (108; Fig. 2G). Alveolar skirts are pronounced (109; Fig. 2G). The first tooth is subincisiform and the succeeding teeth have subconical crowns. In contrast, the first tooth in *A. libratus* is incisiform (110; Fig. 2E), and the crowns of successive teeth are labiolingually compressed. The ventral margin of the antorbital fossa passes caudally along a dorsally convex arc (102; Fig. 2G). The antorbital fenestra is as tall as long (see Russell 1970:fig. 6). The maxillary fenestra is rostrally elongate and dorsoventrally deep (110), forming a strut medial to the rostral fossa margin (Fig. 2G). The promaxillary fenestra lies between these laminae and is dorsally recessed (111; Fig. 2G).

In medial view in *D. torosus* (e.g., CMN 8506), the dental impressions are pit-like (112; Fig. 2K). The dorsal margin of the maxillary antrum passes rostroventrally (113; Fig. 2K), whereas in *A. libratus* the margin is horizontal, beneath which the maxillary fenestra is situated up to half of its height below (114; Fig. 2I). In *D. torosus,* the dorsal margin of the maxillary fenestra approaches (115; Fig. 2K) or extends to the dorsal margin of the antrum. The caudoventral excavation of the maxillary antrum is enlarged and deep (116; Fig. 2K). The floor of the promaxillary recess is crossed by a strut above the third alveolus (117; Fig. 2K).

The palatal process is wide and bounded by a distinct medial ridge; its ventromedial margin passes above the ventral margin of the alveolar process (118; Fig. 2K). The palatine articular surface is a dorsoventrally deep and flat facet (119; Fig. 2K). The tooth root bulges are not visible caudally on the palatal process (120; Fig 2K). The interdental plates are enlarged but unfused (121; Fig. 2K); in some specimens (e.g., AMNH 3456) only the triangular apices of the rostral plates are visible.

Nasal—In Stage 4 *D. torosus* (e.g., CMN 8506) and one *T. rex* specimen (MOR 555), the caudolateral processes are extremely short (Russell, 1970:fig. 6). In *D. torosus,* the nasals are thickened dorsoventrally throughout their length. The caudal plate is over- and underlapped marginally by the lacrimal, and is constricted between the paired bones (122; Fig. 2D). Caudal plate constriction is also seen in *T. bataar* (e.g., PIN 551-2; Maleev, 1974:fig. 3). In *D. torosus,* the lateral margins of the caudal plate are dorsally everted such that the tract rostral to it is dished (123; Fig. 2D). The medial frontal process is elongate (124; Fig. 2D).

In Stage 4 specimens of *T. rex* (e.g., AMNH 5027), the caudal plate is reduced to an elongate rod by the medially expanded lacrimals (Fig. 8C) and the articular surface for the maxilla is a peg-and-socket contact (Fig. 8E).

Lacrimal—In *D. torosus* (e.g., CMN 8506), the cornual process is inflated dorsally and transversely (125; Fig. 3F), broadening its caudal frontal contact, and eliminating the shelf above the ventral ramus (126; Fig. 3F). This inflated condition is also seen in the homologous region of Stage 4 *T. rex* specimens (Fig. 8C, E, I). In *D. torosus,* the cornual process is twice as deep as the lacrimal pneumatic recess (127; Fig. 3F, G). The T-shape of the bone is obscured by the inflated rostral and supraorbital rami (128; Fig. 3F). The rostral margin of the ventral ramus is embayed by the lacrimal recess (129; Fig. 3F). The lacrimal antorbital fossa and the lateral surface of the ventral ramus are sharply separated by the leading edge of the ventral ramus (129; Figs. 3F, G).

The lateral lamina of the rostral ramus appears to be fused with the medial lamina ventrally, rostral to the lacrimal pneu-

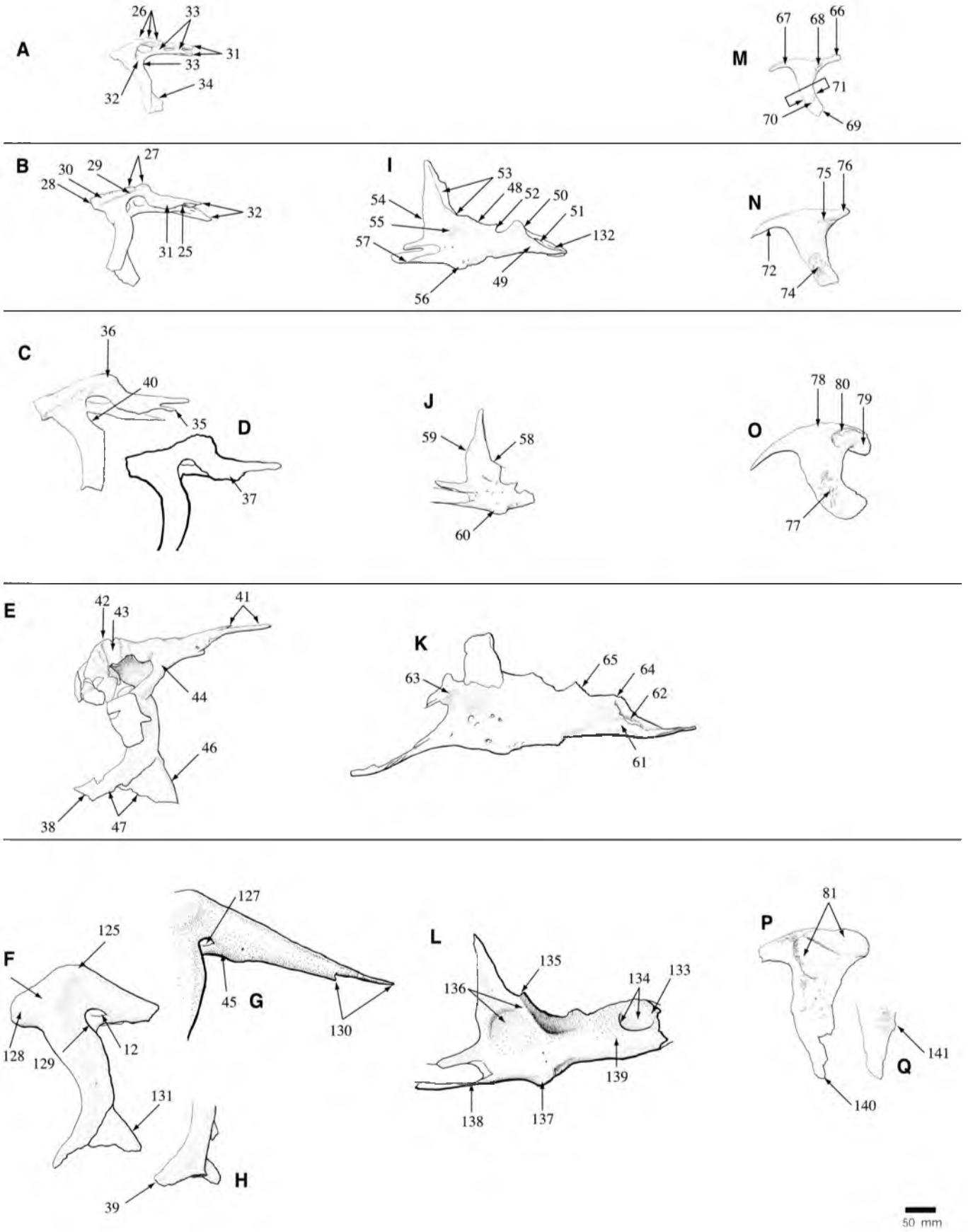

FIGURE 3. Growth series of *Albertosaurus libratus* craniofacial bones: lacrimals in lateral view (TMP 86.144.1, **A**; ROM 1247 **B**; AMNH 5336, **C**, **D**; CMN 2120, **E**); jugals in lateral view (ROM 1247, **I**; AMNH 5336, **J**; CMN 2120, **K**); and postorbitals in lateral view (TMP

matic recess (45; Fig. 3F, G). The dorsal process of the rostral ramus is elongate in contrast to the short ventral process (130; Fig. 3G). The ventral ramus is rostrocaudally broad beneath the dorsal ramus (Fig. 3F). The nasal articular surface is deep and over- and underlaps the bone (CMN 8506). The rostral margin of the rostroventral lamina is straight or convex (131; Fig. 3F). This condition is also in Stage 4 specimens of *T. rex* (Fig. 8E).

Albertosaurus libratus, A. sarcophagus, and *D. torosus* all possess lacrimal cornual processes, in which the cornual process projects rostrodorsally, the apex set rostral or dorsal to the ventral ramus. In *D. torosus,* the rostral ramus is inflated such that the horn is not markedly offset in lateral view. The apex of *A. sarcophagus* is reduced, offset rostrally by a gentle emargination.

In both species of *Tyrannosaurus,* there is no cornual process (Fig. 8C, E, I). Also, the dorsal ramus of Stage 4 specimens is inflated, such that the bone is not dished above the small lacrimal pneumatic recess (Fig. 8E). In Stage 4 *T. rex* specimens, it appears that the medial and lateral laminae of the rostral ramus are fused, and the surface of the latter is excavated laterally by the antorbital fossa and is pierced by two pneumatic foramina (Fig. 8E). In *Albertosaurus* and *D. torosus,* the ventral and dorsal rami meet at a right angle (Figs. 2G–K, 3G–I, 5A). In *Tyrannosaurus,* the ventral ramus meets the dorsal at an acute angle (Molnar, 1991) (Fig. 8E).

Jugal—In *D. torosus* (e.g., CMN 8506), the cleft between the processes of the maxillary ramus curves caudodorsally in lateral view. In *A. libratus,* the cleft is horizontal in lateral view (132; Fig. 3I). The antorbital and secondary fossae of *D. torosus* are separated by a pronounced, rounded septum (133; Fig. 3L) (except TMP 85.62.1). The caudal margin of the jugal pneumatic recess is rebsorbed, fully exposing the secondary fossa in lateral view (134; Fig. 3L). This condition also pertains to *T. rex* (Fig. 8E). The postorbital articular surface is deep and braced ventrally by a bony shelf well dorsal to the ventral margin of the orbit (135; Fig. 3L). The bone is strut-like beneath the postorbital articular surface, producing a deep lateral concavity (136; Fig. 3L); a similar but less pronounced strut and depression are present in *Tyrannosaurus* (e.g., AMNH 5027). The cornual process is prominent and transversely swollen (137; Fig. 3L). The quadratojugal articular surface passes rostrodorsally ahead of the midlength of the ventral process (138; Fig. 3L). The medial articular surface for the lacrimal is braced ventrally by a ridge. Finally, the maxillary ramus is deepened at the level of the jugal pneumatic recess (139; Fig. 3L) and the rostral extremity of the ramus is stout (except TMP 85.62.1).

As in *Albertosaurus* and *D. torosus,* Stage 4 *Tyrannosaurus* specimens bear a low cornual process (Fig. 8C, E, I). In *T. rex,* the contribution of the jugal to the antorbital fenestra is restricted between the maxilla and lacrimal (Fig. 8C, E), unlike the extensive exposure in *Albertosaurus* (Fig. 5A) and *D. torosus* (Russell, 1970:fig. 6).

Postorbital—In *D. torosus* (e.g., CMN 8506), the cornual process may be enlarged to reach or project beyond the dorsal margin of the bone (81; Fig. 3P). The jugal ramus tapers to a point (140). In *A. libratus,* the distal margin of the jugal process is angular in lateral view (69; Fig. 3M). In *D. torosus,* the bone terminates far above the ventral margin of the orbit. Also, a small suborbital prong is present (141; Fig. 3Q). In medial view, the articular surface for the jugal is bipartite and deeply slot-like. The dorsal articular surface for the squamosal terminates caudal to the rostral margin of the laterotemporal fenestra.

In *T. rex* (e.g., AMNH 5027), a dorsal and ventral differentiation of the patch-like cornual process is evident. A rugosity is sometimes developed from its rostral half that proceeds caudally, and may bear a skirt-like ventral ridge (Molnar, 1991). In *Tyrannosaurus,* the suborbital prong is pronounced (Fig. 8C, E, I).

Frontal—In Stage 4 *D. torosus* (e.g., CMN 8506), the paired frontals are as wide as long. In Stage 4 *D. torosus* and *T. rex,* the lacrimal notch is short rostrocaudally and transversely broad caudally (Fig. 8C; Russell, 1970:fig. 6). The frontal slopes ventromedially to meet its counterpart at the midline. The rostral margin of the dorsotemporal fossa extends rostrolaterally and is straightened (Russell, 1970:fig. 7).

In Stage 4 specimens of *T. rex,* the nasal ramus is foreshortened and the dorsotemporal fossa is deep, producing a distinct transverse bar at its rostral margin (Fig. 8C). In some specimens (e.g., TMP 81.6.1) the rostral fossa margin passes caudolaterally in dorsal view. Also in *T. rex,* the paired frontals are wider than each is long (Fig. 8C). The sagittal crest is concave in lateral view and the rostral extent of the crest is cleft sagittally in dorsal view (Fig. 8C).

Prefrontal—In Stage 1 specimens (e.g., ROM 1247) of *A. libratus,* the prefrontal is stout, slightly longer than wide in dorsal view, and does not extend far rostral to the nasal process of the frontal in dorsal view (Fig. 5C).

In small Stage 1 and Stage 4 specimens (e.g., CMN 8506) of *D. torosus,* the prefrontal is several times longer than wide, reaching or extending beyond the nasal process of the frontal rostrally (Russell, 1970:fig. 7). In Stage 4 specimens, the proximal half of the bone is flat and transversely expanded (Russell, 1970:fig. 7).

In Stage 4 *T. rex* specimens, the prefrontal is exposed dorsally as a sliver of bone between the frontal, nasal, and lacrimal (Fig. 8C).

Parietal—In Stage 4 *D. torosus* specimens (e.g., CMN 8506), the nuchal crest is tall, rostrally-everted in lateral view, and dorsolaterally expanded (Russell, 1970:figs. 6, 7). The lateral margins are deeply concave in caudal view. In lateral view, the dorsal margin of the keel-like sagittal crest is deeply concave rostrally. The lateral contact with the frontal is strengthened by a strong transverse ridge (Russell, 1970:fig. 7).

In Stage 4 *T. rex* specimens, the nuchal crest may be rostrocaudally thick and bears a flat and rugose dorsal platform (Fig. 8C, E, G, I). The sagittal crest is transversely thick (Fig. 7C).

Supraoccipital—In Stage 1 specimens (e.g., ROM 1247) of *A. libratus,* the suture with the otoccipital is deeply interdigitating. In Stage 4 *D. torosus* (e.g., CMN 8506) and *T. rex* (e.g., TMP 81.6.1), the suture with the otoccipital may be coalesced. In Stage 4 *T. rex,* the dorsal ramus of the supraoccipital is divided into two processes separated by deep muscle insertions (Fig. 8G), possibly for M. splenius capitis (pers. obs. of *Dromaius novaehollandiae*).

Basioccipital—In Stage 4 *D. torosus* (e.g., CMN 8506), the basioccipital is broadly exposed on the floor of the foramen magnum between the exoccipitals. The ventral surface of the basituberal web is blade-like, as in *T. rex.* The basituberal web may be horizontal in caudal view. The basioccipital is excavated by a deep pit ventral to the neck of the occipital condyle. The basal tuber may be elaborated into a rugose block.

←

86.144.1, **M**; AMNH 5664, **N**; AMNH 5336, **O**). Craniofacial bones of *Daspletosaurus torosus*: lacrimals in lateral view (CMN 8506, **F**; TMP 85.62.1, **G**; CMN 11594, **H**); jugal in lateral view (FMNH PR308, **L**); and postorbitals in lateral view (CMN 11594, **P**; FMNH PR308, **Q**). Arrows indicate features discussed in text. Bones have been reversed to face right when required. Scale bar equals 50 mm; **J** is not to scale.

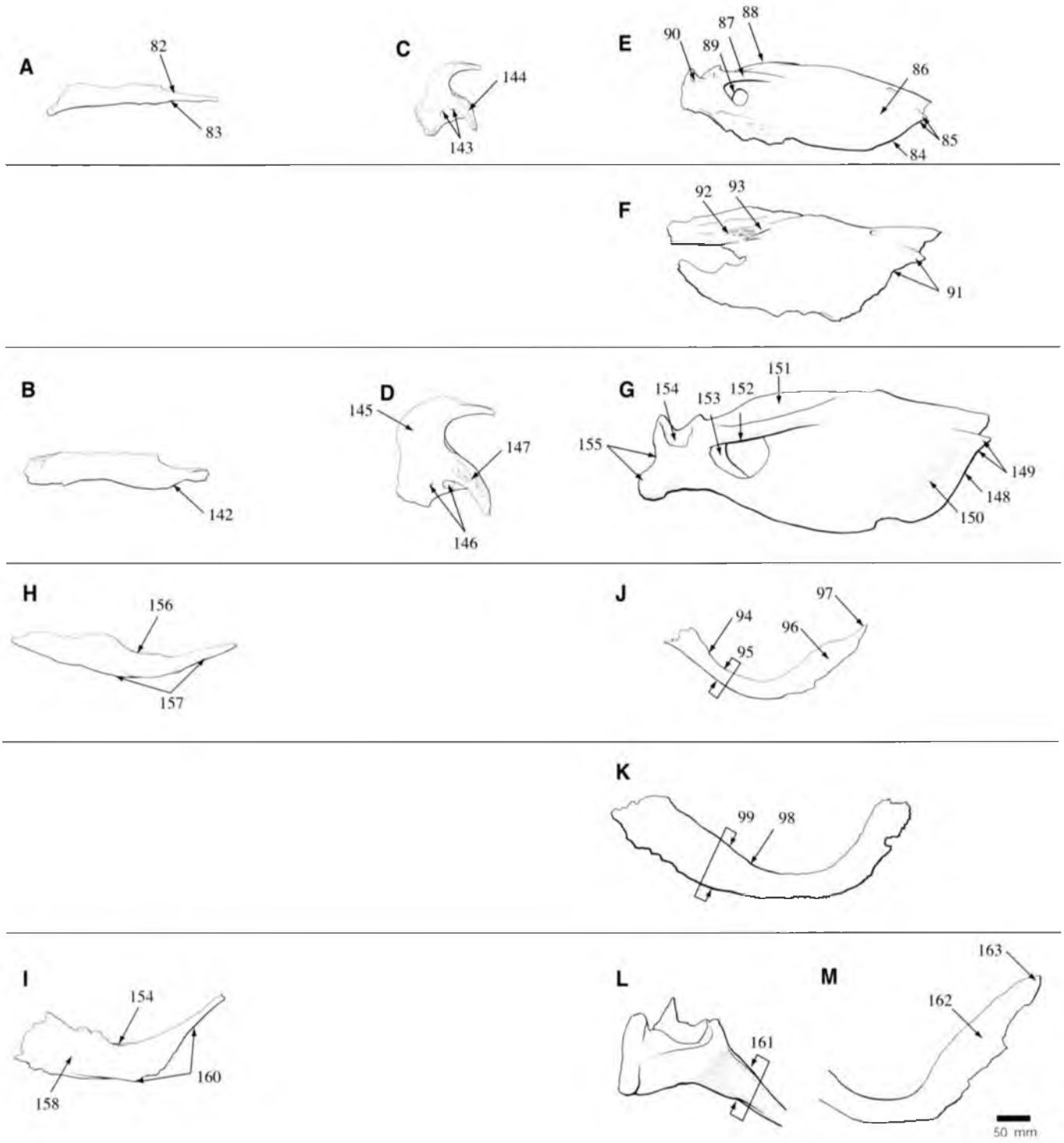

FIGURE 4. Comparison of palatal and mandibular bones: *Albertosaurus libratus* vomer (**A**) in lateral view, ectopterygoid (ROM 1247, **C**) in rostroventral view, growth series of surangulars (ROM 1247, **E**; CMN 2120, **F**) in lateral view, angular (ROM 1247, **H**) in lateral view, and growth series of prearticulars (ROM 1247, **J**; CMN 2120, **K**) in medial view. *Daspletosaurus torosus* vomer (CMN 8506, **B**) in lateral view, ectopterygoid (CMN 8506, **D**) in rostroventral view, surangular (CMN 8506, **G**) in lateral view, angular (CMN 8506, **I**) in lateral view, and prearticular (CMN 8506, **L**, **M**) in medial view. Arrows indicate features discussed in text. Bones have been reversed to face right when required. Scale bar equals 50 mm.

In Stage 4 *T. rex* (e.g., AMNH 5027), the subcondylar recess is shallow (Fig. 8G), induced by the transversely broad and inflated paroccipital region. The recess is occupied by the small, oval basioccipital pneumatic foramen, that pierces the dorsolateral corner of the bone next to the basioccipital-otoccipital suture (Fig. 8G).

Unlike the arcuate suture of other tyrannosaurids, the otoccipital-basioccipital suture of the occipital condyle of the topotype and a referred specimen (ROM 12790) of *A. sarcophagus* is angular in caudal view. The basioccipital separates the otoccipitals from the midline of the condyle by a triangular process. However, the holotype of *A. sarcophagus* displays the condition typical of other tyrannosaurids.

Basisphenoid—In Stage 4 *D. torosus* (e.g., CMN 8506), the rostral margin of the cultriform process curls medially to enclose the space between itself and the rostral surface of the bone. The ventral margin of the bone descends steeply rostroventrally. The basipterygoid facet faces rostrally. The basisphenoid foramina are dorsoventrally elongate and taper dorsally; they are positioned high within the basisphenoid recess. Contra Russell (1970), the presence of a single median pneumatic foramen in the holotype (CMN 8506) is doubtful; the left wall of the recess is crushed medially, obscuring the region of the left foramen completely. In FMNH PR308, the lateral margins of both foramina and a fragment of the median septum between them are visible, the recess in this specimen is otherwise filled with matrix. Further preparation of both specimens is required to clarify structural details.

In Stage 4 *D. torosus,* the oval scar may bear a strongly rugose surface that is convex in transverse section and passes uninterrupted onto the basal tuber. In FMNH PR308 the oval scar is dished and rugose.

In Stage 4 *T. rex* specimens (e.g., AMNH 5027), the rostral plate of the bone is rotated caudally to contact the rostral surface of the basioccipital, eliminating the basisphenoid recess (Fig. 8I). Also, the basisphenoid pneumatic foramina are small and their dorsal margins are at the level of the basioccipital (Fig. 8A, G). The oval scar is concave with a rough surface (Fig. 8 A, G).

In the *A. sarcophagus* specimens CMN 5600 and TMP 86.64.1, each basisphenoid pneumatic foramen lies within a distinct fossa.

Laterosphenoid—In Stage 1 specimens (e.g., ROM 1247) of *A. libratus,* the caudolateral surface is broadly convex in transverse section and gently excavated ventral to the dorsotemporal fossa. The rostrolateral margin is poorly developed, such that the profundus branch of the trigeminal nerve (N. trigeminus) (V) exits rostrally (Russell, 1970).

In Stage 4 *D. torosus* specimens (e.g., CMN 8506), the caudolateral surface is interrupted by a strong, sharp-edged ledge that separates the dorsotemporal fossa from the rostrolateral surface of the bone. The strut-like rostrolateral margin of the bone displaces the exit for the profundus branch of N. trigeminus (V) caudolaterally (Russell, 1970).

Vomer—In Stage 4 *D. torosus* specimens (e.g., CMN 8506), the ventral margin is deep, eliminating the neck-like region in lateral view (142; Fig. 4B). In *D. torosus* and *A. libratus,* the maxillary process is expanded and parallel-sided unlike that of *Tyrannosaurus,* which is diamond-shaped (Fig. 8A; Osborn, 1912)

Ectopterygoid—In Stage 1 specimens (e.g., ROM 1247) of *A. libratus,* the ectopterygoid is dorsoventrally compressed with small, slit-like pneumatic foramina (143; Fig. 4C). The muscle scar on the jugal ramus is caudodorsal in position (144; Fig. 4C).

In Stage 4 *D. torosus* and *T. rex,* the ectopterygoid is inflated (145; Fig. 4D, 8A), with enlarged, rounded pneumatic foramina (146; Figs. 4D, 8A). The muscle scar on the jugal ramus is broad and swollen, and faces ventrally to flank the lateral pneumatic foramen (147; Fig. 4D). In *T. rex* (e.g., MOR 555), the bone is transversely elongate.

Palatine—In Stage 4 *D. torosus* (e.g., CMN 8506), the caudal pneumatic recess is round and there is a broad separation between the recesses. These are also present in the skull of the holotype of *A. sarcophagus,* CMN 5600. In *D. torosus,* the palatine is transversely inflated, a condition seen in the *A. sarcophagus* specimens CMN 5600 and CMN 5601. The palatine is inflated in Stage 4 *T. rex* specimens (e.g., AMNH 5027).

Surangular—In Stage 4 *D. torosus,* the surangular may be deep (148; Fig. 4G). The intramandibular process is deep and stout and meets the rostroventral margin of the surangular at a very low angle or is confluent with the rostroventral margin (149; Fig. 4G). The rostral plate is laterally convex (150; Fig. 4G). The dorsomedial flange may be low or dorsally expanded (151; Fig. 4G). The dorsolateral muscle scar may be rugose rostrally. The surangular shelf is depressed over the surangular foramen (152; Fig. 4G). This condition is also in *T. rex.* The surangular foramen is large and deeply recessed (153; Fig. 4G). The fossa ventrolateral to the glenoid may be dorsoventrally deep or is a rugose pocket (154; Fig. 4G). The caudal margin of the retroarticular process is concave with a caudoventrally projecting heel (155; Fig. 4G).

The surangular of Stage 4 *T. rex* specimens is deep with a subvertical rostral margin and transversely convex rostral plate (Fig. 8E). The dorsomedial flange is low, and the muscle scar lateral to it is rugose. A deep rugose pocket is present lateroventral to the glenoid (Fig. 8E).

Angular—In Stage 1 specimens of *A. libratus,* the bone extends caudal to the surangular foramen (Fig. 5B). The dorsolateral scar passes medial to the caudal plate as a rugose sulcus (156; Fig. 4H). The ventral margin of the rostral process and caudal plate forms a relatively continuous, convex ventral margin (157; Fig. 4H).

In Stage 4 specimens of *D. torosus,* the caudal plate of the bone is dorsoventrally deep (158; Fig. 4I) and may be restricted rostral to the surangular foramen when in articulation (Russell, 1970:fig. 5). It extends caudally in FMNH PR308 (Fig 1; contra Russell, 1970). The dorsolateral scar that passes medial to the caudal flange is strongly pronounced and rugose (159; Fig. 4I). Finally, the rostral process is flexed dorsally relative to the caudal plate (160; Fig. 4I).

In Stage 4 *T. rex* specimens, the angular is deep, the rostral process is flexed relative to the caudal plate (Fig. 8E), extends caudal to the surangular foramen (Fig. 8E; Russell, 1970), and the dorsomedial scar is a pronounced ridge.

Prearticular—In Stage 4 *D. torosus,* the dorsal margin of the deepened caudal ramus is rostral in position and may be developed into a strong keel (161; Fig. 4L); its dorsal and ventral margins may be straightened as they taper rostrally (161; Fig. 4L). The distal margin of the paddle-like rostral lamina (162) may be convex (163; Fig. 4M). These features are also present in Stage 4 *T. rex* (e.g., AMNH 5027).

Splenial—In Stage 1 specimens (e.g., ROM 1247) of *A. libratus,* the rostral extent of the articular surface for the dentary is flat and forms a peg-and-socket contact at its rostral extent. In Stage 4 *D. torosus* (e.g., CMN 8506), the lateral articular surface for the dentary is reinforced by arcuate, interleaving ridges that fit into corresponding slots in the dentary.

Dentary—In Stage 4 *D. torosus* (e.g., CMN 8506), the angular process is dorsoventrally deep. In medial view, the symphysis may be contained rostrally between the rostromedially extending lateral surface and caudally by a pronounced bony ridge. The symphyseal surface is lightly rugose. The articular surface for the splenial extends rostrally, indicated by strong rostroventral ridges and slots. Two to four foramina are present (instead of one or two in *A. libratus*) at the rostral end of the

Meckelian canal. The ventral bar beneath the Meckelian foramina is extremely rugose and transversely convex, obliterating the ventrally passing sulcus. In addition, a low eminence is present at the rostral end of the ventral bar as in *T. rex.*

Dentition

In Stage 1 and Stage 3 specimens of *A. libratus,* the first maxillary tooth is incisiform. In Stage 4 *D. torosus* the first tooth is subincisiform, modified by labiolingual thickening of the tooth. In Stage 1 *A. libratus,* the maxillary teeth are labiolingually compressed and blade-like. The fourth maxillary tooth has a crown width/length ratio of 0.52 (ROM 1247); in Stage 4 *D. torosus,* the teeth are thicker—the crown width/length ratio of the fourth tooth is 0.77 (CMN 8506). In *D. torosus,* the thick maxillary dentition likely increases the depth and width of the alveolar region.

In Stage 1 *A. libratus,* all of the dentary teeth are labiolingually narrow, except for the first. The width/length ratio for the crown of the fourth dentary tooth is 0.5 (ROM 1247); the width/length ratio increases caudally, reaching 0.71 at the 14th tooth. In Stage 4 *D. torosus,* the mesial dentary teeth are labiolingually thick. The crown width/length ratio of the fourth tooth ranges from 0.7 (CMN 8506) to 0.9 (CMN 11594); the distal teeth are also wide, the ratio is 0.73 (CMN 8506).

DISCUSSION

Ontogenetic Variation in *A. libratus*

The growth series of *A. libratus* is divided into three stages; based on the optimal distribution of ontogenetic character states, the growth stages may be characterized as follows. Stage 1 specimens are the least mature, and display nascent ontogenetic states. Stage 2 specimens are typified by the presence of large marginal maxillary neurovascular foramina, a depressed interfenestral strut, an oblique caudal lacrimal suture of the jugal, a postorbital situated dorsal to the orbit floor, a spheroid occipital condyle, a deep surangular, a large and asymmetrical caudal surangular foramen, a lacrimal cornual process with one apex, a dorsolateral lamina of the lacrimal that is as deep as the antorbital fossa, a ventrally oriented and wide oval scar of the basisphenoid, and a deep scar ventrolateral to the glenoid of the surangular. Also, Stage 2 specimens may exhibit nascent Stage 1 features.

Stage 3 specimens are characterized by an antorbital fenestra in which the height approaches the length, an expansive rostrolateral surface of the maxilla, a convex rostral margin of the rostroventral lamina of the lacrimal, a deep maxillary process of the jugal, and elongate rostral processes of the dorsal ramus of the lacrimal. In Stage 3, all small Stage 1 features are transformed but large Stage 1 and Stage 2 features may be unmodified.

Tyrannosaurid Taxonomy

Evidence for ontogenetic changes in the skull and mandible of *Albertosaurus libratus* (Lambe, 1914) provides parameters by which similar variation in other tyrannosaurid crania may be inferred. As such, inference of a pattern of ontogenetic change in one taxon requires verification in another. The morphological changes in the face, from an early to a late ontogenetic stage, is an alternative hypothesis to interpretations of tyrannosaurid diversity in which sympatric tyrannosaurid taxa are seen as comprising a giant and dwarf, or more lightly built taxon (e.g., Russell, 1970; Molnar, 1980; Currie, 1987; Bakker et al., 1988; Paul, 1988; Carpenter, 1992). This hypothesized pattern requires further examination.

Nanotyrannus lancensis

CMNH 7541, a damaged skull with lower jaws in occlusion (Fig. 6A–D), was collected from the Hell Creek Formation of Montana in 1942 and described by C. W. Gilmore (1946) in a posthumous publication. CMNH 7541 was heavily restored in plaster, and Gilmore erred in his account of sutural fusion in the skull, a misinterpretation perpetuated by later workers (Russell, 1970; Bakker et al., 1988; Paul, 1988). In fact, there is no evidence of sutural fusion in this specimen except for fusion of the intranasal and intraparietal sutures, which is typical of Stage 1 *A. libratus.* Gilmore noted the similarity of the skull to the smallest specimen of *A. libratus* then known (AMNH 5664); thus Gilmore (1946) made CMNH 7541 the holotype of the new taxon, *Gorgosaurus lancensis.*

In his review of tyrannosaurids from western Canada, Russell (1970) referred "*G*". *lancensis* to *Albertosaurus* and accepted Gilmore's interpretation of sutural fusion and its indication of relative maturity. Later, Bakker et al. (1988:17) proposed a new genus of dwarf tyrannosaurid, *Nanotyrannus,* for "*G.*" *lancensis,* offering sutural fusion between the frontal and prefrontal and between the parietal and frontal as the criteria for the adult nature of the specimen.

Relative Maturity of CMNH 7541

The presence of striated cortical bone was demonstrated by Bennett (1993) and Sampson (1993) to distinguish immature, fast-growing individuals from mature specimens for pterosaurs and centrosaurine ceratopsids, respectively. Immature bone grain is lost with increase in size and development of ontogenetic characters, thus providing a crude measure of relative maturity among reptiles.

On CMNH 7541, immature bone grain is present on the antorbital fossa of the maxilla (Fig. 7A) and lacrimal, lateral surface of the vomer, dentary, surangular (Fig. 7C), angular, palatine, jugal (Fig. 7B), ventral process of the maxilla, quadratojugal process of the squamosal, squamosal ramus of the postorbital, rostral surface of the supraoccipital crest of the parietal, medial surface of the prearticular and splenial, caudal margin of the quadratojugal, caudal surface of the quadrate, and dorsal surface of the frontal and nasals (Fig. 7D).

In addition, none of the "fusions" (frontal–frontal, frontal–prefrontal, nasal–maxilla, nasal–lacrimal, nasal–prefrontal, premaxilla–maxilla, maxilla–lacrimal, maxilla–nasal) claimed by Gilmore (1946) or by Bakker et al. (1988) actually occurs in CMNH 7541. In fact, none of the fusions enumerated above occurs in any tyrannosaurid skulls externally (pers. obs.), except suture closure around the prefrontal varies in some *T. rex* (Brochu, pers. comm.). Therefore, I regard CMNH 7541 as a Stage 1 specimen on the basis of cortical bone texture, a conclusion consistent with its size (skull length 572 mm). Also, CMNH 7541 exhibits the characters typical of Stage 1 specimens of *A. libratus* (see Appendix 1).

Premaxilla—In rostral view, the premaxillae are narrow and their lateral margins are concave at the base of the maxillary processes, and the alveolar region is shallow (Fig. 8J).

Maxilla—The maxillae of CMNH 7541 are laterally flattened, the alveolar process is shallow, the first tooth is incisiform, and the remaining teeth are labiolingually narrow (Fig. 6A, D). Also, the ventrolateral rim of the ventral jugal process is not breached by the caudalmost neurovascular sulcus of the ventral row of foramina (Fig. 6A). The lateral surface does not extend caudally over the rostral margin of the antorbital fossa (Fig. 6A), the promaxillary fenestra is dorsoventrally elongate and not recessed (Fig. 6A), the antorbital fenestra is longer than high, and the small maxillary fenestra is midway between the rostral margins of the antorbital fossa and restored fenestra (Fig. 6A).

Nasal—In CMNH 7541, the nasals are smooth with low transverse and fine rostrocaudal ridges (Fig. 6A, B). In the smallest Stage 1 specimen of *A. libratus* examined (TMP 86.144.1), the rugose texture typical of mature specimens is present. The condition in CMNH 7541 might represent individual, ontogenetic, or taxonomic variation.

Lacrimal—In CMNH 7541 the rostral margin of the rostroventral lamina is concave to straight and the contact of the lamina with the jugal exceeds that of the ventral ramus as in Stage 1 *A. libratus* (Fig. 6A). Also, there is no evidence of fusion between the ventral margins of the medial and lateral processes of the rostral ramus.

Jugal—As in Stage 1 *A. libratus,* the maxillary ramus of CMNH 7541 is dorsoventrally shallow and tapered (Fig. 6A). The jugal pneumatic recess is a rostrally-restricted slit (Fig. 6A), the postorbital articular surface approaches the orbit floor (Fig. 6A), the region ventral to the postorbital ramus is convex (Fig. 6A), the caudal margin of the postorbital ramus is convex at midheight, and the caudal rim of the lacrimal articular surface is subvertical (Fig. 6A).

Postorbital—As in Stage 1 *A. libratus,* the laterodorsal margin is not everted medially into the dorsotemporal fenestra (Fig. 6A, B). There is no postorbital cornual process or suborbital prong (Fig. 6A); the former is represented by a textured surface. Unlike *A. libratus,* the rostral and caudal margins of the jugal process taper rostroventrally (Fig. 6A).

Prefrontal—As in Stage 1 *A. libratus* specimens, the prefrontal is situated at the rostrolateral margin of the frontal, bounded caudally by a triangular, tab-like process from the frontal to separate it from the lacrimal caudolaterally (Fig. 6B).

Frontal—As in Stage 1 *A. libratus,* the lacrimal notch in CMNH 7541 is elongate and narrow in dorsal view, the prefrontal notch is rostrocaudally stout in dorsal view, and the paired frontals are longer than wide (Fig. 6B). Further evidence of the immature nature of the specimen is provided by the relatively elongate orbital margin (11 mm) and the shallow dorsotemporal fossa, which has a barely discernible rostral margin (Fig. 6B). Unlike Stage 1 *A. libratus,* the frontals appear to rise to meet each other along the midline rostral to the dorsotemporal fossa (Fig. 6B); however, cracks suggest this may be an artifact of dorsoventral crushing.

Parietal—In CMNH 7541 the delicate nuchal crest is low in caudal view (Fig. 6C). Its dorsal margin is rostrally everted and the laterodorsal margin is convex in frontal section (Fig. 6A, B). Unlike Stage 1 *A. libratus,* the sagittal crest in lateral view is tall and blade-like.

Ectopterygoid—In CMNH 7541, unlike Stage 1 *A. libratus,* the ectopterygoid is inflated, except for the jugal ramus (Fig. 6D). As in Stage 1 *A. libratus,* the muscle scar on the jugal ramus is caudolaterally positioned.

Supraoccipital—As in Stage 1 *A. libratus,* the dorsal process of the supraoccipital of CMNH 7541 is narrow and has a horizontal dorsal border with flange-like rostrolateral edges (Fig. 6C).

Basioccipital—As in Stage 1 *A. libratus,* the ventrolateral margins of the occipital condyle taper toward each other ventrally and the caudoventral condylar surface is flattened (Fig. 6C). The ventral surface of the basituberal web is flat and arched in caudal view (Fig. 6C). The median portion of the basioccipital is concave between the laminae and the bone is strongly excavated caudolaterally by the subcondylar recess (Fig. 6C).

Parabasisphenoid—As in Stage 1 *A. libratus,* the pneumatic foramina in the basisphenoid are small and situated ventrally and the oval scar is smooth and lateroventrally oriented (Fig. 6C, D).

Dentary—As in Stage 1 *A. libratus* the dentary of CMNH 7541 is relatively shallow in lateral view and narrow in ventral view (Fig. 6A, D).

Surangular—In CMNH 7541 the surangular is shallow and the surangular shelf is horizontal (Fig. 6C).

Prearticular—As in Stage 1 *A. libratus* the dorsal margin of the caudal ramus of the prearticular is restricted caudally (Fig. 6D), the caudal ramus is shallow with parallel dorsal and ventral margins (Fig. 6D), the rostral lamina is slightly expanded and its parallel margins converge to a point distally (Fig. 6D), and the caudodorsal surface of the rostral lamina is smooth (Fig. 6D).

CONCLUSIONS

Immaturity of CMNH 7541

The morphological structure of CMNH 7541 agrees with that of Stage 1 specimens of *A. libratus* and displays no mature features. The weight of evidence indicates that CMNH 7541 is juvenile. The presence of immature bone grain (Fig. 7) precludes the specimen from representing an adult pygmy tyrannosaurid.

Status of *Nanotyrannus*—Rozhdestvensky (1965) first suggested that CMNH 7541 might be a juvenile *Tyrannosaurus rex,* based on his observations of *T. bataar,* in which juveniles vary in "slightly different proportions than in the large specimens, as we should expect if they are of different (ontogenetic) ages" (Rozhdestvensky, 1965:106).

Carpenter (1992) also suggested that CMNH 7541 might be an immature specimen of *T. rex* on the basis of its long and low snout, separate nasals and frontal, circular orbit, and rostrocaudally oval margin of the antorbital fenestra. Carpenter was uncertain of the significance of the last feature, owing to its acute rostral margin relative to that in immature specimens of *T. bataar.* In fact, on both sides, this region is absent and restored in plaster in CMNH 7541. Carpenter's suggestion concerning ontogenetically variable features, except for the nasal–frontal contact, is consistent with the observations reported here. He noted two features that united the specimen with *Tyrannosaurus*: considerable lateral constriction of the snout, and a dorsally broad temporal region (Fig. 8C, D). However, Carpenter (1992:528) tentatively accepted Russell's identification of CMNH 7541 as ?*A. lancensis.*

CMNH 7541, and specimens referred to *T. rex,* share the following characters: (1) nasal processes of the premaxillae tightly appressed throughout their entire length (Fig. 8I, J); (2) restricted exposure of the jugal within the antorbital fenestra (Fig. 8E, F); (3) antorbital fossa reaches the nasal suture caudodorsally (Fig. 8E, F); (4) transversely broad jugal pneumatic recess (Fig. 8C, D); (5) elongate frontal sagittal crest (Fig. 8C, D); (6) strongly divergent and short basal tubers (Fig. 8G, H); (7) rostroventrally-oriented caudal occipital plate (Fig. 8A, B); (8) shallow subcondylar recess (Fig. 8G, H); (9) rostroventrally deep basisphenoid plate and rostrocaudally-restricted basisphenoid recess (Fig. 8A, B, G, H); (10) inflated ectopterygoid (Fig. 8A, B); (11) strongly convex rostral plate of the surangular (Fig. 8E, F); (12) transversely narrow snout and broad temporal region relative to other tyrannosaurids (Fig. 8C, D) (Carpenter, 1992); and (13) deep mandible relative to other tyrannosaurids (Fig. 8E, F). Given the low number of specimens of *T. bataar* examined first-hand for this study, it is conceivable that some of these characters may be generic synapomorphies. Based on the close morphological similarities between the skull of CMNH 7541 and large *T. rex* skulls, I thus consider *Nanotyrannus lancensis* Bakker et al., 1988 a subjective junior synonym of *Tyrannosaurus rex* Osborn, 1905.

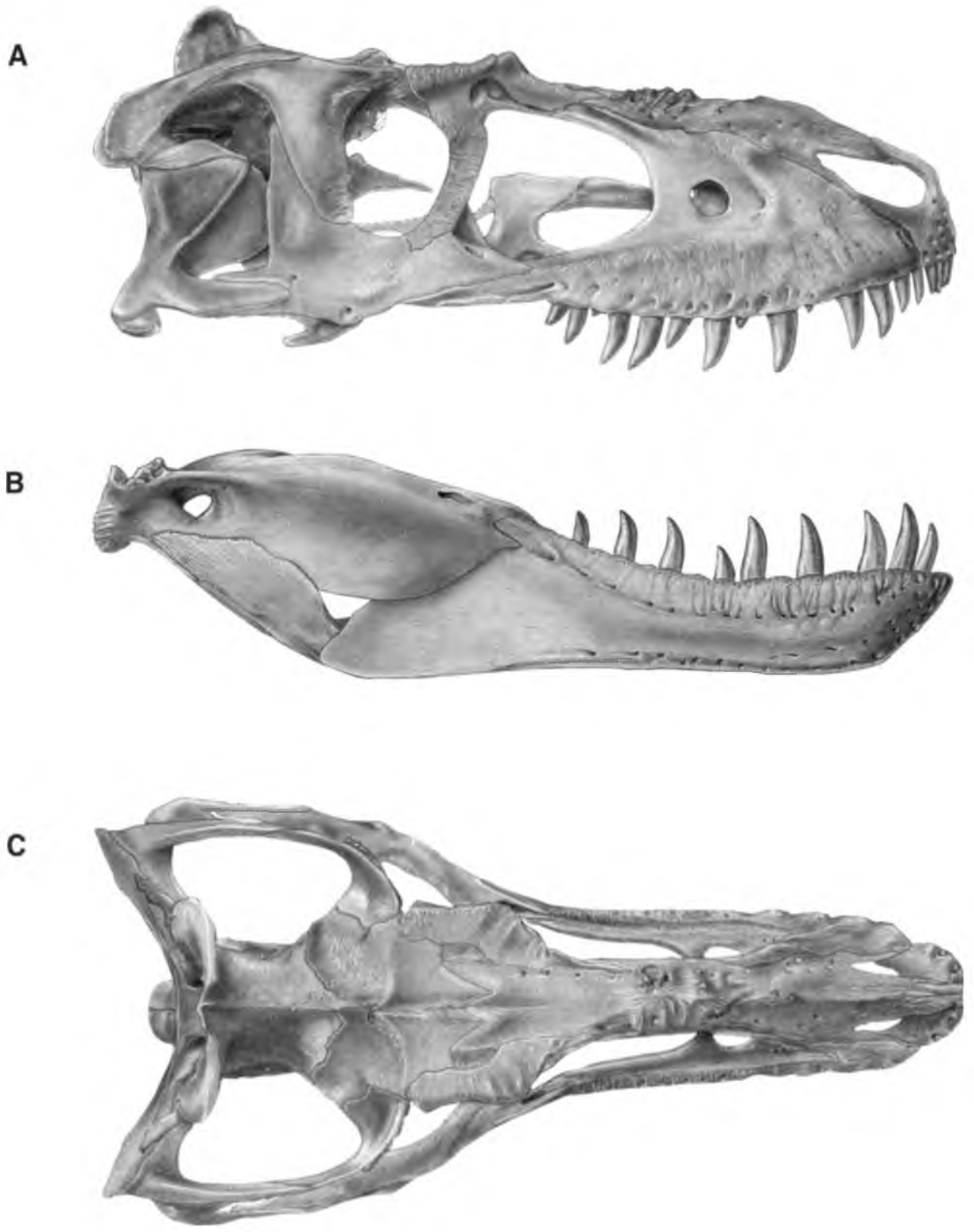

FIGURE 5. Composite (AMNH 5664, CMN 11315, ROM 1247, TMP 91.36.500, USNM 12815) early ontogeny (large Stage 1) skull and jaw of *Albertosaurus libratus* in lateral (**A**, **B**) and dorsal (**C**) views. Skull length approximately 750 mm.

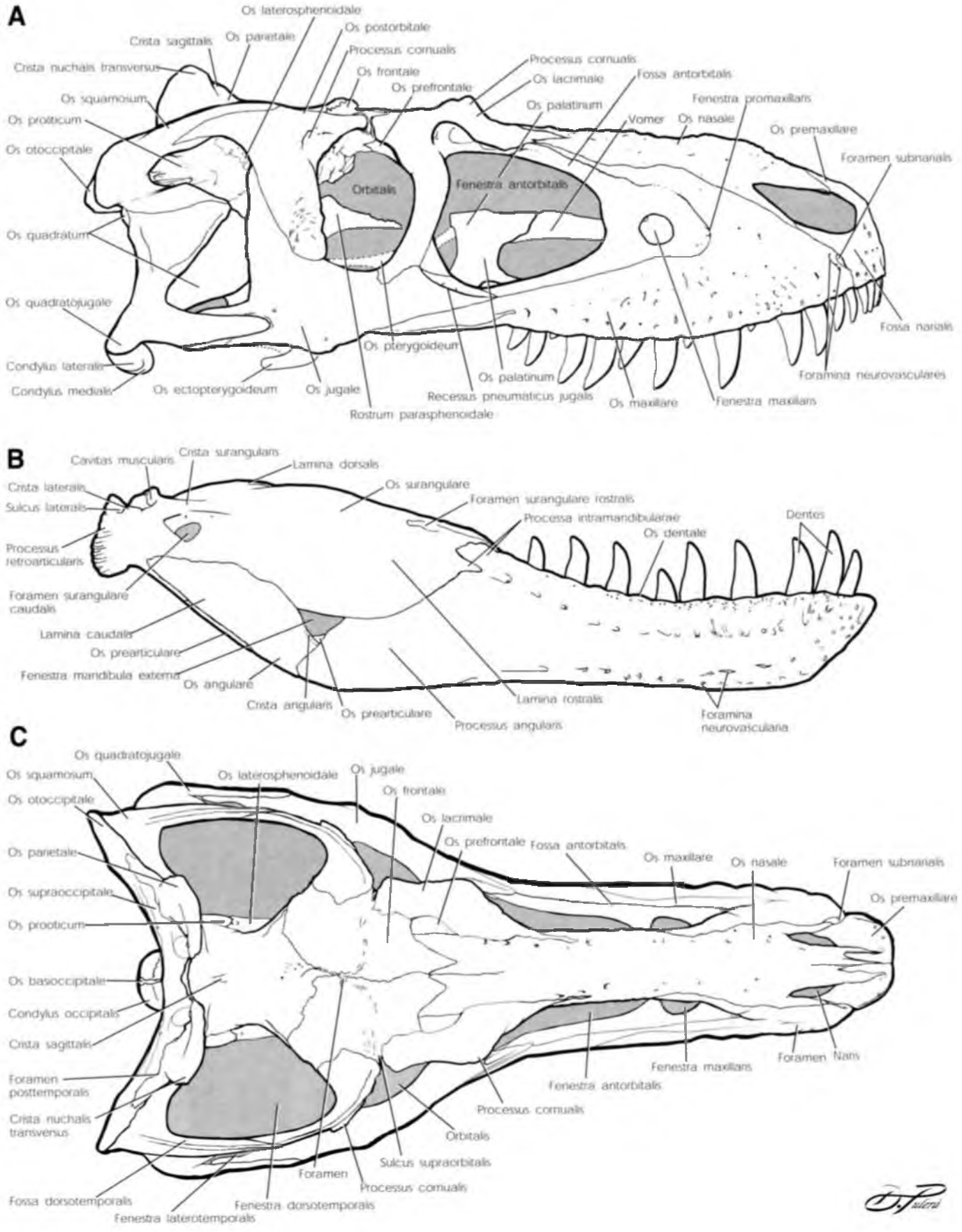
A
Os laterosphenoidale
Os postorbitale
Crista sagittalis
Os parietale
Processus cornualis
Crista nuchalis transversus
Os frontale
Processus cornualis
Os lacrimale
Fossa antorbitalis
Os squamosum
Os prefrontale
Os palatinum
Fenestra promaxillaris
Os prooticum
Vomer
Os nasale
Os premaxillare
Os otoccipitale
Foramen subnarialis
Orbitalis
Fenestra antorbitalis
Os quadratum
Os quadratojugale
Fossa narialis
Os pterygoideum
Condylus lateralis
Os palatinum
Foramina neurovascularia
Condylus medialis
Os ectopterygoideum
Os jugale
Recessus pneumaticus jugalis
Os maxillare
Fenestra maxillaris
Rostrum parasphenoidale
B
Cavitas musculoris
Crista surangularis
Lamina dorsalis
Crista lateralis
Os surangulare
Sulcus lateralis
Foramen surangulare rostralis
Processus intramandibulares
Dentes
Os dentale
Processus retroarticularis
Foramen surangulare caudalis
Lamina caudalis
Os prearticulare
Fenestra mandibula externa
Os angulare
Crista angularis
Os prearticulare
Lamina rostralis
Processus angularis
Foramina neurovascularia
C
Os quadratojugale
Os squamosum
Os laterosphenoidale
Os jugale
Os otoccipitale
Os frontale
Os lacrimale
Os parietale
Os prefrontale
Fossa antorbitalis
Os maxillare
Os nasale
Foramen subnarialis
Os supraoccipitale
Os premaxillare
Os prooticum
Os basoccipitale
Condylus occipitalis
Crista sagittalis
Foramen Nars
Fenestra maxillaris
Foramen posttemporalis
Fenestra antorbitalis
Crista nuchalis transversus
Processus cornualis
Orbitalis
Sulcus supraorbitalis
Foramen
Processus cornualis
Fossa dorsotemporalis
Fenestra dorsotemporalis
Fenestra laterotemporalis

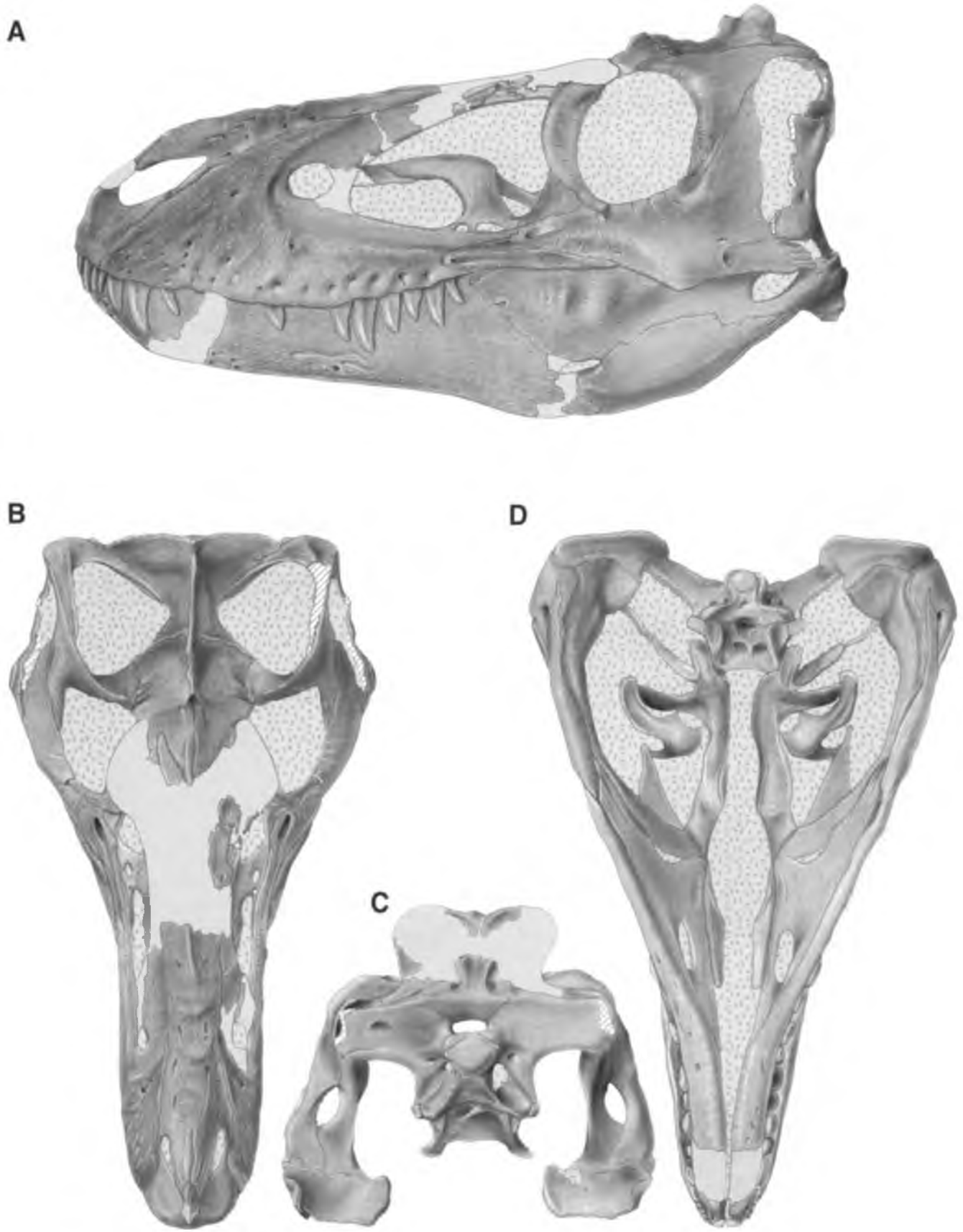

FIGURE 6. Restored skull with occluded jaws of a Stage 1 *Tyrannosaurus rex* (CMNH 7541) in left lateral (**A**), dorsal (**B**), occipital (**C**), and palatal (**D**) views. Skull length is 572 mm. Rostral and transverse crushing of the suspensorium in **A** and **B** has not been corrected. Basisphenoid pneumatic foramina are restored in **D**; right squamosal is restored in **B**; occipital condyle is restored in **C**. **Abbreviations**: **ang**, os angulare; **ar**, os articulare; **bo**, os basioccipitale; **bs**, os basisphenoidale; **bs rec cl**, basisphenoid recess ceiling; **co**, os coronoideum; **cr sag**, crista sagittalis; **dn**, os dentale; **ect**, os ectopterygoideum; **imf**, fenestra intramandibulare; **ipv**, vacuita interpterygoideum; **la**, os lacrimale; **mx**, os maxillare; **na**,

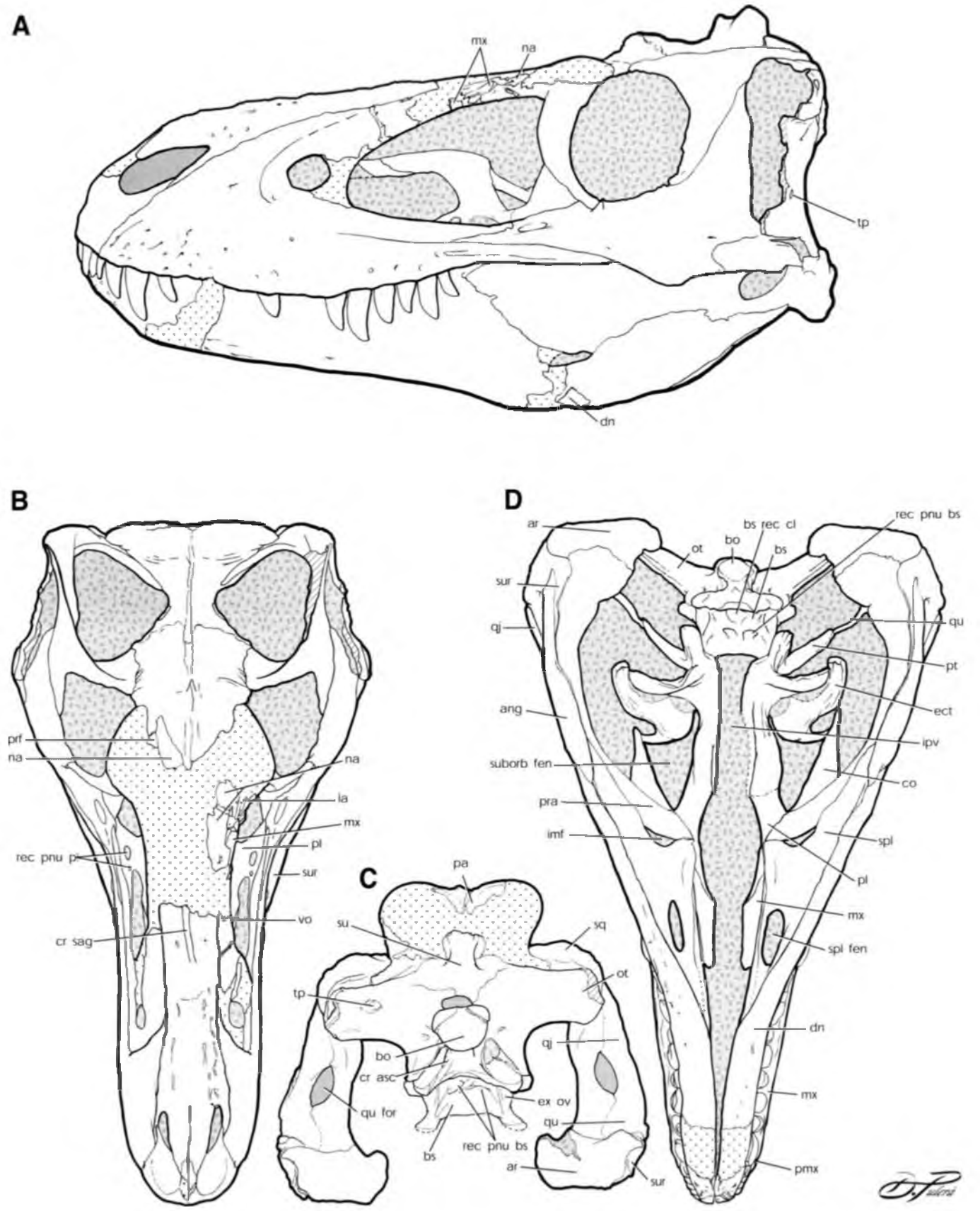

FIGURE 6. Continued os nasale; **ot**, os otoccipitale; **pa**, os parietale; **pl**, os palatinum; **pmx**, os premaxillare; **pra**, os prearticulare; **prf**, os prefrontale; **pt**, os pterygoideum; **qj**, os quadratojugale; **qu**, os quadratum; **qu for**, foramen quadratum; **rec pnu bs**, recessus pneumaticum basisphenoidale; **rec pn pl**, recessus pneumaticum palatinum; **sq**, os squamosum; **spl**, os spleniale; **spl fen**, fenestra spleniale; **suborb fen**, fenestra suborbitalis; **sur**, os surangulare; **tp**, tooth puncture; **vo**, vomer.

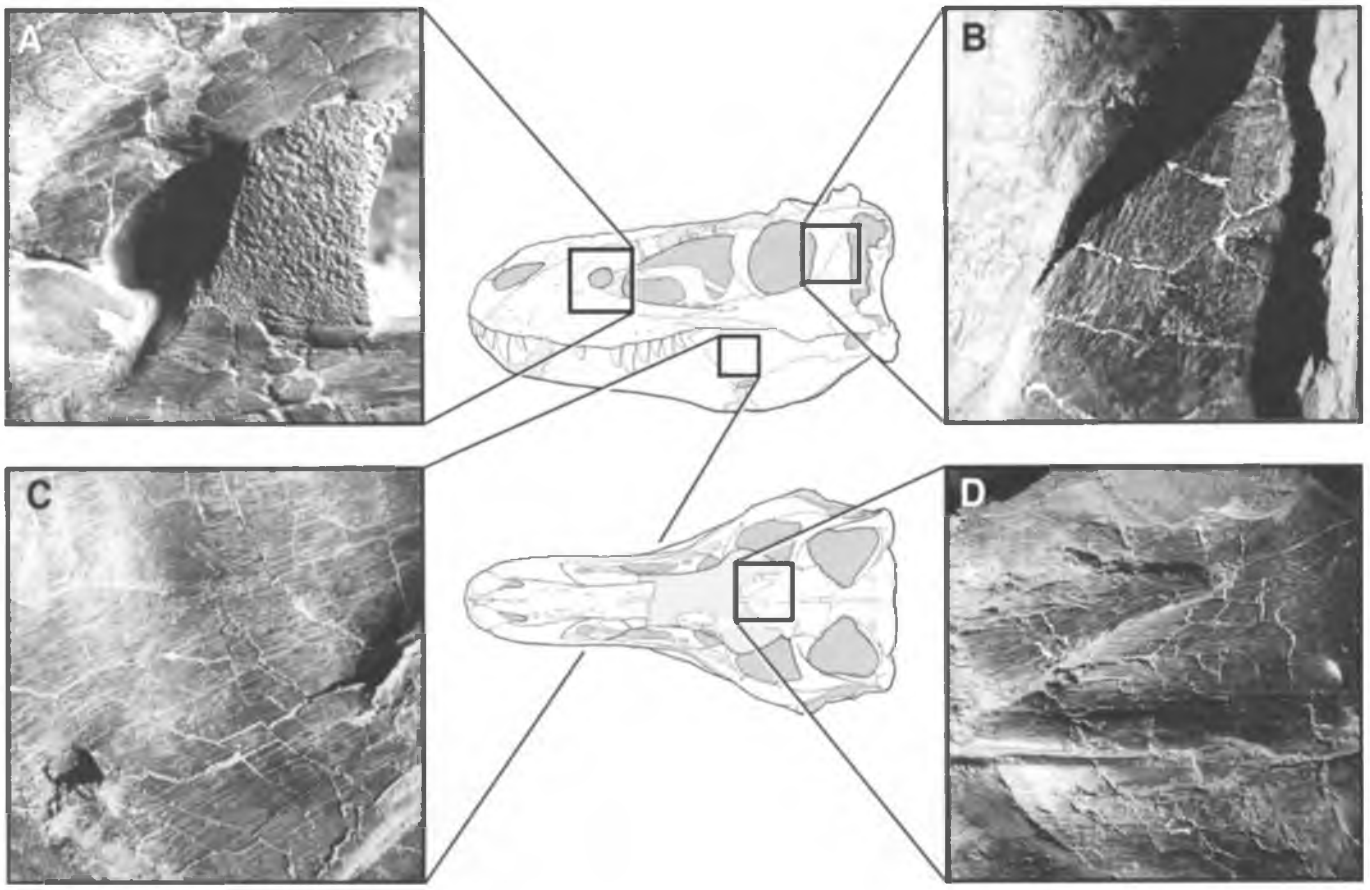

FIGURE 7. Immature bone grain on the lateral surface of the antorbital fossa of the maxilla (**A**; reversed), jugal (**B**), surangular (**C**), and the dorsal surface of the nasal and frontal (**D**) of an early ontogeny *Tyrannosaurus rex* (CMNH 7541). Skull length is 572 mm.

Ontogeny in *Tyrannosaurus rex*

Ontogeny in the craniofacial skeleton of *Tyrannosaurus rex* is characterized by a global shift from a gracile early ontogeny to a robust late ontogeny morphotype. In *T. rex* the rostral maxillary and dentary teeth become conical, expanding and deepening the alveolar processes of the maxilla and dentary (Fig. 8A, C, E, F). The tooth row becomes rostrodorsally reoriented, and the teeth become procumbent (Bakker et al., 1988). Also, the maxilla loses three to four teeth from the rostral end of the tooth row, because the rostral teeth undergo the greatest change. Although tooth count has been used to distinguish tyrannosaurid taxa (e.g., Bakker et al., 1988), caution is advised because counts appear to be sensitive to ontogenetic and individual variation.

A similar pattern of loss of tooth positions is present in the maxilla of *A. libratus,* dropping from 16 to 13 alveoli (Table 2). Although one large Stage 1 specimen (USNM 12814) has a low alveolus count, this specimen is the most mature of the growth stage (Carr, in prep.). While loss of alveoli may be individually variable, it is evident that the phenomenon occurs in mature specimens (Table 2). Among other archosaurs, ontogenetic tooth loss has been reported by Mook (1921), Wermuth (1953), and Iordansky (1973) in *Crocodylus cataphractus, C. porosus, C. siamensis,* and *Tomistoma schlegelii.* This indicates that ontogenetic tooth loss among Tyrannosauridae is not withXout precedent among Archosauria.

In agreement with Molnar's detailed functional analysis (1973), the adult skull of *T. rex* is constructed for forceful biting. In *T. rex,* the dorsotemporal fossa becomes deeply excavated during ontogeny, reflecting hypertrophied adductor musculature (Fig. 8C, D). The entire skull is modified to accommodate the change, including the rostrally-oriented orbits (Fig. 8C, D, I, J). In concert with the increase in bite force, the muzzle and jaws become deep and contacts between bones are strengthened by peg-and-socket sutures, such as the nasomaxillary contact (Fig. 8E). The facial skeleton is buttressed to deliver and absorb the resultant forces of increased bite force, evidenced by the strut-like rostral margin of the antorbital fossa, which passes to the columnar dorsum of the snout. Also, the premaxillary dental arcade of early growth stages is abandoned for a sparser arrangement of teeth (Fig. 8I, J), indicating the less specialized grasping function characteristic of the remainder of the rostral maxillary tooth row.

In addition, the craniofacial air sac system (sensu Witmer, 1987, 1990, 1997) had a primary role in modifying bone structure. The antorbital air sac rested within the antorbital fenestra and antorbital fossa, sending diverticula into the ectopterygoid, palatine, lacrimal, jugal, and maxilla. As maturity was attained, the diverticula invaded the bones more fully, expanding the sinuses and bones. Combined with changes induced by an enlarged dentition, late ontogeny specimens became 'swollen-faced' relative to their smaller, sleeker progeny. It is probable that the swollen bones had greater cross-sectional strength than the strap-like bones of smaller animals, a morphological shift that would be important for taking live prey.

Finally, pneumatic features indicate further ontogenetic

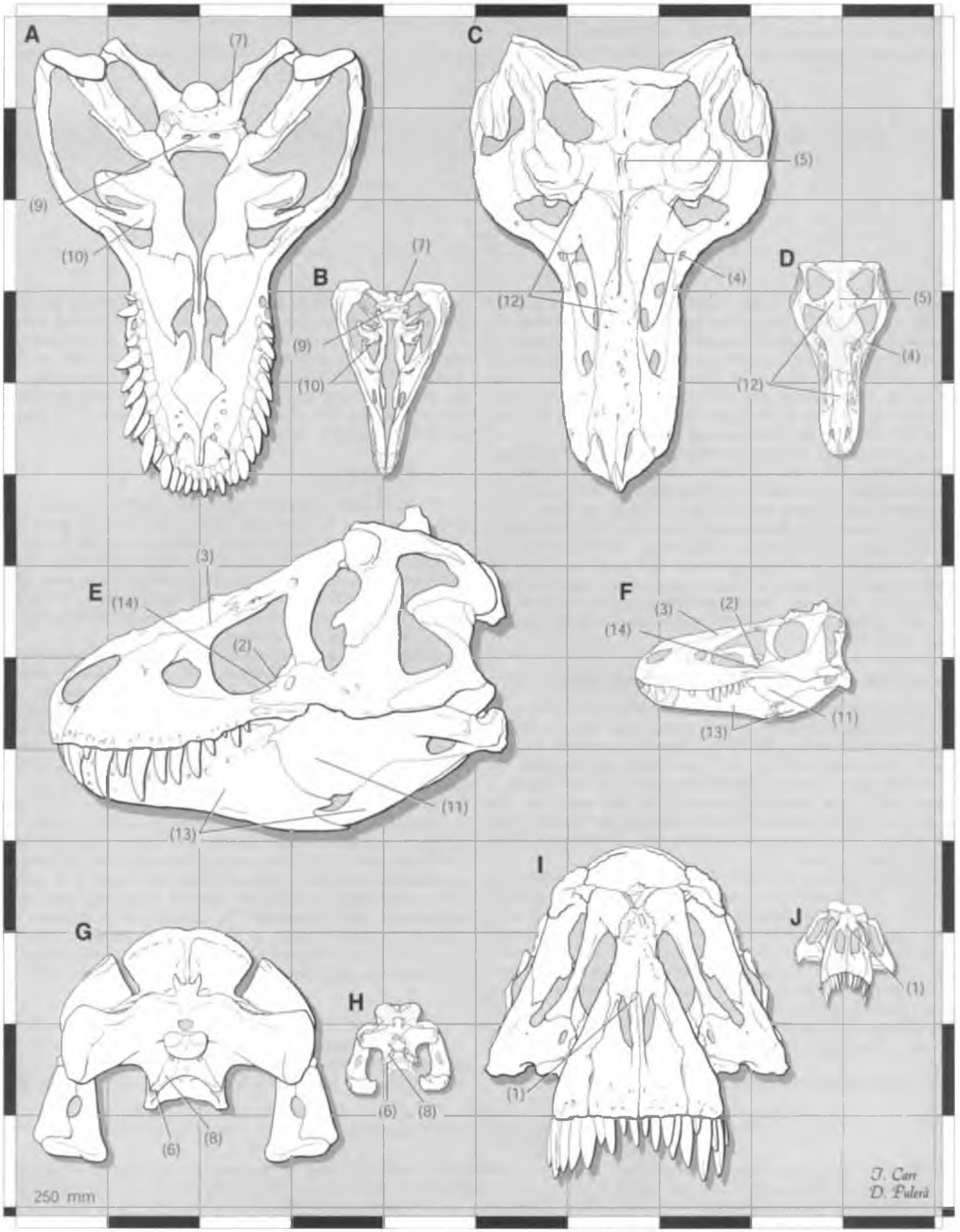
A
(7)
(9)
(10)
B
(7)
(9)
(10)
C
(5)
(4)
(12)
D
(5)
(4)
(12)
E
(3)
(14)
(2)
(11)
(13)
F
(3)
(2)
(14)
(11)
(13)
G
(6)
(8)
H
(6)
(8)
I
(1)
J
(1)
250 mm
J. Carr
D. Fulera

TABLE 2. Maxillary tooth counts of maxillary alveoli, growth stage, and skull lengths of *Albertosaurus libratus* specimens showing a tendency for more mature specimens to have fewer tooth positions. () = estimated.

Specimen	Stage	# Maxillary alveoli	Skull length (mm)
AMNH 5664	1	15 (Bakker et al., 1988)	678 (Russell, 1970)
ROM 1247	1	14 (pers. obs.)	(750) (pers. obs.)
USNM 12814	1	13 (Bakker et al., 1988)	(795) (Russell, 1970)
TMP 83.36.100	1	15 (pers. obs.)	—
CMN 2270	1	15 (pers. obs.)	—
CMN 12063	1	14 (pers. obs.)	—
AMNH 5336	2	13 (Bakker et al., 1988)	(962) (Bakker et al., 1988)
UA 10	3	13 (Currie, pers. comm.)	(900) (Currie, pers. comm.)
AMNH 5458	3	14 (pers. obs.)	990 (Russell, 1970)
CMN 2120	3	13 (pers. obs.)	1,000 (pers. obs.)

change in *T. rex*. The Stage 4 specimens CM 9380, LACM 23844, and UCMP 118742 share maxillary fenestrae that are rostrodorsally deep and extend medial to the rostral margin of the antorbital fossa to a greater degree than in other specimens (e.g., AMNH 5027, BHI 2033, TMP 81.6.1, MOR 555). In addition, the interfenestral strut is thin, and additional pneumatic foramina are present at the apex (CMN 9380) or at the base (LACM 23844) of the interfenestral strut.

It is evident that the distinct structural patterns of early and late ontogeny specimens of *T. rex* constrained their respective foraging behaviors, which in late ontogeny individuals appears specialized to grasp and hold live prey or to dismember a large carcass. Alternatively, the changes represent a reaction norm to the size of the skull, increased bite forces, and increased prey size. Nonetheless, it is not improbable that small and large animals differed in foraging strategy, consumption technique, and/or prey type. Such size dependent differences are found in extant crocodilians (Grenard, 1991) and monitor lizards (Auffenberg, 1988, 1994).

Maleevosaurus novojilovi and *Tyrannosaurus bataar*

PIN 552-2 was originally described by Maleev (1955a) as *G. novojilovi*. Rozhdestvensky (1965) recognized this specimen as a juvenile of *T. bataar*. In 1992, Carpenter proposed the new genus, *Maleevosaurus* for "*G.*" *novojilovi*, arguing that the small maxillary fenestra, promaxillary fenestra not visible in lateral view, large antorbital fenestra, low lacrimal horn, low postorbital cornual process, shallow maxilla, and slender jugal fall outside of the range of variation seen in juveniles of *A. libratus* and *T. bataar*.

Maleev's published figure (1974:fig. 55) of the skull indicates that PIN 552-2 conforms to the features characteristic of early ontogeny *A. libratus*: delicate nasal with a slotted maxilla suture, long antorbital fenestra, round maxillary fenestra positioned midway between the interfenestral strut and rostral margin of the antorbital fossa, promaxillary fenestra not recessed, rostral margin of the antorbital fossa not overlapped by the lateral surface, shallow alveolar process of the maxilla, shallow and delicate jugal (Carpenter, 1992), low postorbital cornual process (Carpenter, 1992), and shallow dentary (Carpenter, 1992).

As in late ontogeny specimens of *T. bataar* (Maleev, 1974: figs. 1, 48), there is no lacrimal cornual process, the maxillary fenestra is relatively large, and the postorbital cornual process is patch-like. Because of the incompleteness of the specimen, the number of diagnostic features to be gleaned from an illustration is limited. However, in the absence of apomorphies and on geographic and stratigraphic grounds, it is most parsimonious to consider PIN 522-2 as a young specimen of *T. bataar*, as first suggested by Rozhdestvensky (1965).

Overall Conclusions

Tyrannosaurid craniofacial ontogeny follows a conservative pattern that can be observed across taxa. The recognition of ontogenetic variation reduces the number of sympatric taxa and renders the concept of dwarf tyrannosaurids untenable. Immature tyrannosaurids have been misidentified as pygmy adults (e.g., Maleev, 1974; Gilmore, 1946; Bakker et al., 1988; Carpenter, 1992). Small skulls and mandibles are delicate in contrast to the robust large specimens.

An additional source of confusion is the resemblance of early ontogeny tyrannosaurid skulls to those of adult small theropods. A tyrannosaurid skull 37% of maximum length has an orbit 17% of its skull length. Adult small theropods have similar, if not identical, proportions (e.g., *Coelophysis bauri*, CM C-4-81; skull length 250 mm; orbit/skull length ratio 16%) (Colbert, 1989). In contrast, in small theropods, small crania 35% of maximum adult length have relatively enlarged orbits (e.g., *C. bauri*, MCZ 4326; skull length approx. 88 mm; orbit skull length ratio 34%) (Colbert, 1989). The comparable proportions of early ontogeny tyrannosaurids with adult small theropods may have misled previous workers. Although the immature tyrannosaurids examined herein are not hatchlings, it is perhaps noteworthy that they lack the enlarged orbits and short snouts of juvenile small theropods. It is possible that hypotheses concerning particular modes of heterochrony might be generated to explain the phenomenon. In this case, acceleration and hypermorphosis might be invoked (sensu Reilly et al., 1997).

ACKNOWLEDGMENTS

This paper is the result of research begun as a fourth-year undergraduate thesis under the supervision of Dr. H.-D. Sues and culminating in a Master's thesis while at the University of

←

FIGURE 8. Comparison of Stage 1 (CMNH 7541) and Stage 4 (AMNH 5027, MOR 555) skulls of *Tyrannosaurus rex* in palatal (**A**, **B**), dorsal (**C**, **D**), lateral (**E**, **F**), caudal (**G**, **H**), and rostral (**I**, **J**) views. Numbered labels indicate *T. rex* autapomorphies: (1) nasal processes of the premaxillae tightly appressed throughout their entire length; (2) restricted exposure of the jugal within the antorbital fenestra; (3) antorbital fossa reaches the nasal suture caudodorsally; (4) transversely broad jugal pneumatic recess; (5) elongate frontal sagittal crest; (6) strongly divergent and short basal tubers; (7) rostroventrally-oriented caudal occipital plate; (8) shallow subcondylar recess; (9) rostroventrally deep basisphenoid plate and rostrocaudally-restricted basisphenoid recess; (10) inflated ectopterygoid; (11) strongly convex rostral plate of the surangular; (12) transversely narrow snout and broad temporal region relative to other tyrannosaurids; and (13) deep mandible relative to other tyrannosaurids.

Toronto. I thank the remainder of my Master's committee, Drs. M. Gagnon, C. McGowan, and R. Winterbottom, for reviewing the original thesis on which this paper is based. I gratefully acknowledge the constructive reviews of the manuscript by Drs. L. M. Witmer (Ohio University, Athens) and C. A. Brochu (Field Museum, Chicago).

For providing access to specimens in their care, I thank P. J. Currie (Royal Tyrrell Museum of Palaeontology), M. Norell (American Museum of Natural History), D. A. Russell (North Carolina State University, Raleigh), K. L. Seymour (Royal Ontario Museum), K. Shepherd (Canadian Museum of Nature), W. Simpson (Field Museum of Natural History), M. Williams (Cleveland Museum of Natural History), and L. M. Witmer. For stimulating discussions on various aspects of this project, I thank R. Heinrich (Ohio University, Athens), and L. M. Witmer. Thanks also to Ms. E. LeBlanc for a helpful question which improved the manuscript. I thank Dr. P. J. Currie for graciously sharing unpublished information and providing comments on an earlier version of this manuscript. Funding for part of this research was provided by NSF Grant IBN-9601174 to L. M. Witmer. Partial support for page charges was provided by Dr. H.-D. Sues.

For supplying casts I thank M. Fair and P. May of Research Casting International (*A. libratus, T. rex*). For their logistical support throughout this project, I thank C. Crinnion (McMaster University), R. Day (Canadian Museum of Nature), M. Ellison (American Museum of Natural History), G. Jackson (Cleveland Museum of Natural History), C. Kennedy (Canadian Museum of Nature), I. Morrison (Royal Ontario Museum), and T. Samman (University of Toronto).

Line drawings for Figures 5, 6, and 7 were skillfully executed by Mr. Dino Pulerà. The dedicated work, talent, and skill of Dino on the carbon-dust plates deserve special mention. All other figures are by the author. Special thanks go to Dino and his wife, Cinzia, for providing the opportunity to see this final phase of the project to its end. In memoriam Peter David James Jacobs (1967–1997).

LITERATURE CITED

Auffenberg, W. 1988. Gray's Monitor Lizard. University of Florida Press, Gainsville, 419 pp.

——— 1994. The Bengal Monitor. University Press of Florida, Gainsville, 560 pp.

Bakker, R. T., M. Williams, and P. J. Currie. 1988. *Nanotyrannus*, a new genus of pygmy tyrannosaur, from the latest Cretaceous of Montana. Hunteria 1:1–30.

Baumel, J. J., and L. M. Witmer. 1993. Osteologia; pp. 45–132 *in* J. J. Baumel, A. S. King, J. E. Brezile, H. E. Evans, and J. C. Vanden Berge (eds.), Handbook of Avian Anatomy: Nomina Anatomica Avium, 2nd ed. Club. Cambridge, Massachusetts.

Bennett, S. C. 1993. The Ontogeny of *Pteranodon* and Other Pterosaurs. Paleobiology 19:92–106.

Brochu, C. A. 1996. Closure of neurocentral sutures during crocodilian ontogeny: implications for maturity assessment in fossil archosaurs. Journal of Vertebrate Paleontology 16:49–62.

Carpenter, K. 1992. Tyrannosaurids (Dinosauria) of Asia and North America; pp. 250–268 *in* N. Mateer and P. J. Chen (eds.), Aspects of Nonmarine Cretaceous Geology. China Ocean Press, Beijing.

Carr, T. D. 1996. Cranial osteology and craniofacial ontogeny in Tyrannosauridae (Dinosauria: Theropoda) from the Dinosaur Park Formation (Judith River Group, Upper Cretaceous: Campanian) of Alberta. M.Sc. thesis, University of Toronto, 358 pp.

Currie, P. J. 1987. Theropods of the Judith River Formation of Dinosaur Provincial Park, Alberta, Canada; pp. 52–60 *in* P. J. Currie and E. H. Koster (eds.), Fourth Symposium on Mesozoic Terrestrial Ecosystems, Short Papers. Occasional Papers, Tyrrell Museum of Palaeontology, 3.

Gilmore, C. W. 1946. A new carnivorous dinosaur from the Lance Formation of Montana. Smithsonian Miscellaneous Collections 106:1–19.

Grenard, S. 1991. Handbook of Alligators and Crocodiles. Krieger Publishing Company, Malabar, Florida, 210 pp.

Holtz, T. R., Jr. 1994a. The phylogenetic position of the Tyrannosauridae: implications for theropod systematics. Journal of Palaeontology 68:1100–1117.

——— 1996. Phylogenetic taxonomy of the Coelurosauria (Dinosauria: Theropoda). Journal of Paleontology 70:536–538.

Iordansky, N. N. 1973. The skull of the Crocodilia; pp. 201–262 *in* C. Gans and T.S. Parsons (eds.), Biology of Reptilia, Vol. 4. Academic Press, New York.

Lambe, L. M. 1914. On a new genus and species of carnivorous dinosaur from the Belly River Formation of Alberta, with a description of the skull of *Stephanosaurus marginatus* from the same horizon. The Ottawa Naturalist 28:158–164.

Leidy, J. 1856. Notice of remains of extinct reptiles and fishes, discovered by Dr. F. V. Hayden in the badlands of the Judith River, Nebraska Territory. Proceedings of the Academy of Natural Sciences of Philadelphia 8:72–73.

Makovicky, P. J., and P. J. Currie. 1998. The presence of a furcula in tyrannosaurid theropods, and its phylogenetic and functional implications. Journal of Vertebrate Paleontology 18:143–149.

Maleev, E. A. 1955a.[New carnivorous dinosaurs from the Upper Cretaceous of Mongolia.] Doklady Akademia Nauk SSSR 104:779–782. [Russian.]

——— 1955b.[A giant meat-eating dinosaur from Mongolia.] Doklady Akademii Nauk SSSR 104:634–637. [Russian.]

——— 1974. [Giant carnosaurs of the Family Tyrannosauridae.] [Transactions of the Joint Soviet-Mongolian Paleontological Expedition] 1:132–191. [Russian, English Summary]

Matthew, W. D., and B. Brown. 1922. The family Deinodontidae, with notice of a new genus from the Cretaceous of Alberta. Bulletin of the American Museum of Natural History 46:367–385.

——— and ——— 1923. Preliminary notices of skeletons and skulls of Deinodontidae from the Cretaceous of Alberta. American Museum Novitates 89:1–9.

Molnar, R. E. 1973. The cranial morphology and mechanics of *Tyrannosaurus rex* (Reptilia: Saurischia). Ph.D. dissertation, University of California, Los Angeles, 451 pp.

——— 1980. An albertosaur from the Hell Creek Formation of Montana. Journal of Paleontology 54:102–108.

——— 1991. The cranial morphology of *Tyrannosaurus rex*. Palaeontographica, A, 217:137–176.

Mook, C. C. 1921. Individual and age variation in the skulls of recent Crocodilia. Bulletin of the American Museum of Natural History 64:51–66.

Osborn, H. F. 1905. *Tyrannosaurus* and other Cretaceous carnivorous dinosaurs. Bulletin of the American Museum of Natural History 21:259–265.

——— 1912. Crania of *Tyrannosaurus* and *Allosaurus*. Memoirs of the American Museum of Natural History 1:1–30.

Paul, G. S. 1988. Predatory Dinosaurs of the World: A Complete Illustrated Guide. Simon and Schuster, New York, 464 pp.

Reilly, S. M., E. O. Wiley, and D. J. Meinhardt. 1997. An integrative approach to heterochrony: the distinction between interspecific and intraspecific phenomena. Biological Journal of the Linnean Society 60:119–143.

Rozhdestvensky, A. K. 1965. Growth changes in Asian dinosaurs and some problems of their taxonomy. Palaeontological Journal 3:95–109.

Russell, D. A. 1970. Tyrannosaurs From the Late Cretaceous of Western Canada. National Museum of Natural Sciences Publications in Palaeontology 1:1–30.

Sahni, A. 1972. The vertebrate fauna of the Judith River Formation, Montana. Bulletin of the American Museum of Natural History 147:232–412.

Sampson, S. D. 1993. Cranial Ornamentations in Ceratopsid Dinosaurs: Systematic, Behavioral, and Evolutionary Implications. Ph.D. dissertation, University of Toronto, Toronto, 299 pp.

Sereno, P. C. 1997. The origin and evolution of dinosaurs. Annual Review of Earth and Planetary Sciences 25:435–489.

Wermuth, H. 1953. Systematik der rezenten krokodile. Mitteilungen der Zoologische Museum Berlin 29:375–514.

Witmer, L. M. 1987. The nature of the antorbital fossa of archosaurs: shifting the null hypothesis; pp. 234–239 *in* P. J. Currie and E. M. Koster (eds.), Fourth Symposium on Mesozoic Terrestrial Ecosys-

tems. Short Papers. Revised ed. Occasional Paper of the Tyrrell Museum of Palaeontology, 3.

——— 1990. The craniofacial air sac system of Mesozoic birds (Aves). Zoological Journal of the Linnean Society 100:327–378.

——— 1997. The evolution of the antorbital cavity of archosaurs: a study in soft-tissue reconstruction in the fossil record with an analysis of the function of pneumaticity. Society of Vertebrate Paleontology Memoir 3:1–73; supplement to Journal of Vertebrate Paleontology 17(1).

Received 1 June 1998; accepted 5 January 1999.

APPENDIX 1. A genus-level comparison of tyrannosaurids: the growth changes of *Albertosaurus libratus* compared with the homologous characters in *Daspletosaurus torosus* and *Tyrannosaurus rex*. Abbreviations: **aofen**, antorbital fenestra; **aofo**, antorbital fossa; **artic**, articular; **basis pn for**, basisphenoid pneumatic foramen; **cdrsl**, caudodorsal; **cnflt**, confluent; **cnvx**, convex; **corn**, cornual; **dtf**, dorsotemporal fossa; **fen**, fenestra; **hrz**, horizontal; **intramnd**, intramandibular; **ltfen**, laterotemporal fenestra; **M. add mand ext**, Musculus adductor mandibular pars externus; **max**, maxilla; **occ con**, occipital condyle; **pn**, pneumatic; **po**, postorbital; **pr**, process; **qj**, quadratojugal; **rd**, rostrodorsal; **rv**, rostroventral; **sbn**, subnarial; **shllw**, shallow; **smth**, smooth; **sq**, squamosal; **surf**, surface.

Albertosaurus libratus Stage 1	Stage 2	Stage 3	*D. torosus* Stage 4	*T. rex* Stage 1	Stage 4
Premaxilla					
Transversely narrow	narrow	wide	wide	narrow	wide
Concave lateral margin	—	straight	straight	concave	straight
Shallow alveolar process	shallow	shallow	deep	shallow	deep
Narrow maxillary process	—	wide	wide	narrow	wide
Alveolar skirts absent	absent	absent	present	absent	present
Dorsal flange on palatal process absent	—	—	present	—	—
Caudal crest ventral to subnarial foramen absent	—	—	present	—	—
Max. pr. does not overlap sbn. pr. of nasal broadly	narrow	narrow	narrow	broad	broad
Maxilla					
Transversely compressed	thick	thick	thick	compressed	thick
Dorsolateral nasal facet	—	dorsal	dorsomedial	dorsal	dorsomedial
Distinct antorbital fossa (small) grades rostroventrally (large)	grades	grades	grades	grades	grades
Ventral margin aofo concave or straight	sigmd/cnvx	—	convex	straight	concave/straight
Interfenestral strut flat (small) concave (large)	flat	concave	concave	flat	concave
Long antorbital fenestra	long	round	round	long	round
Rostrolateral foramina small	large	large	large	small	large
Ridge ventral to aofo	—	—	absent	present	absent
Shallow alveolar process	shallow	shallow	deep	shallow	deep
Flat or convex premaxillary process	—	—	swollen	—	swollen
Ventral rostral foramen small	large	large	large	—	large
Dorsal rostral foramen a cleft	round	round	round	—	round
Caudal sulcus above ventral margin	breaches	breaches	breaches	above	breaches
Maxillary fenestra midway in position	rostral	rostral	rostral	midway	rostral
Maxillary fenestra circular	elongate	elongate	elongate	circular	elongate
Shallow tab between nasal suture and antorbital fossa	shallow	shallow	deep tab	absent	absent
Promaxillary fenestra slitlike	recessed	slit/recess	foramen	slit	foramen
Shallow rostrolateral surface	expanded	expanded	expanded	shallow	expanded
Depression below aofo deep	shallow	shallow	absent	shallow	absent
Aofo rostral margin indistinct	strut	strut	strut	indistinct	strut
Shallow maxillary antrum fossae	—	—	variable	—	deep
Caudoventral fossa shallow or deep	—	—	deep	—	shallow
Low ridge across promaxillary antrum floor	—	—	strut	—	ridge
Dorsal surface of palatal process visible	—	—	not visible	—	visible
Ventral edge of palatal process ventrally everted	—	—	level	—	raised
Palatine articular surface cleft-like	—	—	flat facet	—	coarse facet
Palatal process narrow	—	—	wide	—	wide
Shallow interdental impressions	—	—	pit-like	—	shallow
First tooth incisiform	—	incisiform	subincisiform	incisiform	subconical
Nasal					
Lightly built	thick	thick	thick	light	thick
Moderately or strongly vaulted	moderate	moderate	moderate	moderate	moderate
Medial frontal process absent (small) or present (large)	absent/present	present	elongate	—	elongate
Caudal plate expands slightly between lacrimals	expands	parallel	constricted	—	constricted
Marginal lacrimal overlap	marginal	marginal	extensive	—	extensive
Coarse dorsal surface	coarse	coarse	coarse	smooth	coarse
Maxillary contact slotted	—	slotted	peg socket	—	peg socket
Caudolateral process elongate	elongate	elongate	short	—	variable
Caudal plate tract shallow	shallow	shallow	dished	—	dished
Lacrimal					
Ventral pr. of rostral ramus absent (small) incipient (large)	short	long	short	—	long
Cornual process a weak ridge (small) pronounced apex (large)	apex	apex	apex	—	absent
Cornual process with three apices (small) two apices (large)	one	one	one	—	absent

APPENDIX 1. *(Continued)*

Albertosaurus libratus Stage 1	Stage 2	Stage 3	*D. torosus* Stage 4	*T. rex* Stage 1	Stage 4
Cornual process rostrodorsal	rostrodorsal	erect	variable	—	absent
Corn. pr. lower than lacrimal fen. (small), or deep as lacrimal fenestra (large)	deep	deep	deeper	—	deeper
Bone is T-shaped	T-shaped	T-shaped	T-shaped	7-shaped	7-shaped
Rostrolateral margin of corn. pr. eave-like	eave-like	eave-like	inflated	—	inapplicable
Supraorbital pr. ridge absent (small) or present (large)	present	present	inflated	—	inflated
Surface around aofen dished	dished	not dished	not dished	—	not dished
Dorsolateral lamina absent (small) dorsolateral lamina present but low (large)	deep as aofo	fused	fused	unfused	fused
Aofo and lateral surface merge	—	edge	edge	merge	merge
Rostral margin of lamina concave or straight	—	convex	cnvx/straight	straight	convex
Jugal articular surface exceeds that of ventral ramus	—	equal	equal	exceeds	equal
Caudal margin of jugal contact subvertical	caudodorsal	caudodorsal	caudodorsal	subvertical	caudodorsal
Rostral margin of ventral ramus not embayed by aofen	embayed	embayed	embayed	not embayed	not embayed
Dorsal pr. of rostral ramus present	present	present	elongate	—	present
Jugal					
Caudodorsally declined po. pr. (small), or erect (large)	erect	erect	erect	erect	erect
Orbital margin level and elongate	—	level/elongate	cdrsl/concave	level	concave
Maxillary process shallow	—	deep	deep	shallow	deep
Jugal pneumatic recess a narrow slit	slit	slit	slit	wide	wide
Caudal edge of recess united with or merged beneath lacrimal	—	merge	merge	merge	merge
Caudal edge of pr. resorbed (small) or not resorbed (large)	not resorbed	resorbed	resorbed	not resorbed	resorbed
po. artic. surf. to orbit floor	dorsal	dorsal	dorsal	floor	dorsal
Overlapping medial lacrimal artic. surf	—	—	shelf-like	—	—
Caudal margin of po. pr. sinuous or concave	cnvx/straight	—	sinuous	sinuous	sinuous/straight
Lateral surface flat or convex beneath po. pr.	convex	concave	pocket	convex	concave
Cornual pr. narrow	narrow	narrow	wide	narrow	wide
Cornual pr. pronounced or low	pronounced	low	pronounced	pronounced	variable
qj. articular surface at or caudal to midlength of qj. pr.	—	—	rostral	rostral	rostral
qj. articular surface ventral margin horizontal or rostrodorsal	rostrodorsal	rostrodorsal	rostrodorsal	rostrodorsal	horizontal
Cleft between max. prs. horizontal	horizontal	horizontal	caudodorsal	—	—
Contribution to aofen extensive	extensive	extensive	extensive	limited	limited
Postorbital					
Frontal pr. elongate (small) short (large)	short	short	short	elongate	short
Frontal process shallow	deep	deep	deep	shallow	deep
Squamosal pr. slender	deep	—	deep	slender	deep
Cornual process a depression (small), or tab (large)	knob	boss	boss	irregular surf	boss
Jugal ramus elongate and slender	broad	broad	broad	slender	broad
Jugal articular surface shallow	—	—	cleft	—	—
Rostral and caudal margins of jugal process parallel distally	converge	converge	taper	taper	taper
Dorsotemporal fossa shallow (small) or deep (large)	deep	deep	deep	shallow	deep
dtf not bounded by a ridge (small) low ridge present (large)	present	present	present	present	present
sq. pr. ventral margin concave (small) sinuous (large)	concave	—	variable	sinuous	sinuous
Dorsal margin of bone vertical	everted	—	everted	vertical	everted
Squamosal articular surface rostral to ltfen	rostral	rostral	caudal	rostral	rostral
Suborbital process absent	absent	absent	present	absent	present
Frontal					
Orbital margin within a vertical slot	slot	slot	slot	margin	slot
Lacrimal notch long and narrow	—	—	short/wide	long/narrow	short/wide
Paired frontals longer than wide	—	—	width=length	width<length	width>length
Dorsotemporal fossa shallow	deep	deep	deep	shallow	deep
Frontals flat to meet at midline	dorsomedial	dorsomedial	ventromedial	flat	flat
Prefrontal articular surface narrow in dorsal view	narrow	—	wide	narrow	wide
Rostral margin of dtfo arcuate	arcuate	arcuate	straight	arcuate	backswept
Parietal					
Nuchal crest low in caudal view	low	tall	tall	low	tall
Lateral surface of nuchal crest rugose	dorsal	—	—	smooth	dorsal
Low sagittal crest	deep	—	deep	deep	deep
Basioccipital					
Occ. con. caudoventrally flat	spherical	—	spherical	flat	spherical
Lateral margins of occ. con. converge ventrally	round	—	round	converge	round
Ventral surface of basituberal web flat and arched	flat, arched	—	blade level	flat arched	blade level
Bone ventral to occ. con. convex	convex	concave	concave	?convex	flat
Basal tuber poorly developed	rugose	—	rugose	smooth	rugose

APPENDIX 1. *(Continued)*

Albertosaurus libratus Stage 1	Stage 2	Stage 3	*D. torosus* Stage 4	*T. rex* Stage 1	Stage 4
Basisphenoid					
Basipterygoid process flat rostrolaterally	—	—	rostral	—	—
Basis. pn. for. small and ventral	small, ventral	—	deep dorsal	small ventral	large dorsal
Ventral margin of bone slopes at a low angle	low	steep	steep	low	steep
Oval scar smooth	smooth	—	coarse	smooth	coarse
Oval scar ventromedial	ventromedial	ventromedial	ventral	lateroventral	variable
Oval scar narrow	wide	wide	wide	narrow	wide
Vomer					
Slender neck between palatine and pmx prs.	—	—	deep convex	—	—
Palatine					
Caudal pn. recess elongate	—	—	round	round	round
Bone laterally compressed (small) inflated (large)	inflated	inflated	inflated	inflated	inflated
Shallow vomer process	deep	—	deep	intermediate	intermediate
Surangular					
Fossa lateral to glenoid absent (small) shallow and smooth (large)	deep rugose	—	deep rugose	shllw smth	deep rugose
Caudal margin of retroarticular process concave (small) straight to convex (large)	—	concave	concave	concave	concave
Bone shallow	deep	deep	deep	shallow	deep
Intramandibular process stout and deep	—	elongate	stout deep	—	stout deep
Intramnd. pr. and plate joined by shallow curve or confluent	angle	angle	angle/cnflnt	confluent	confluent
Rostral plate flat	flat	flat	convex	convex	convex
Surangular shelf slants rostroventrally or horizontally	hrz/rv/rd	rostrodorsal	hz/rd	—	horizontal
Lateral margin of shelf projects lateroventrally	horizontal	lateroventral	depressed	horizontal	depressed
Dorsomedial pr. low and bladelike or tall	—	tall	variable	—	low
Indistinct M. add. mand. ext. scar	—	inset	coarse	—	coarse
Caudal surangular foramen small	large	large	large	small	large
Caudal surangular foramen round	asymmetrical	asymmetrical	asymmetrical	round	asymmetrical
Prearticular					
Lateral angular facet aliform (small) flat, not aliform (large)	—	flat	flat	—	flat
Dorsal margin caudal	—	rostral	rostral	caudal	rostral
Shallow caudal ramus	—	deep	deep	shallow	deep
Straplike rostral lamina	—	—	paddlelike	straplike	paddlelike
Caudodorsal margin smooth	—	scarred	scarred	smooth	scarred
Dentary					
Bone wide as deep (small) deeper than wide (large)	depth>width	depth>width	depth>width	depth>width	depth>width
Angular process shallow	deep	deep	deep	shallow	deep
Symphyseal surface flat	—	flat/rugose	flat/rugose	—	flat
Splenial facet with light ridges	—	—	deep	—	—